*minerals*

MDPI

*Article*

# Corona-Type Textures in Ultrabasic Complexes of the Serpentinite Belt, Kola Peninsula, Russia

**Andrei Y. Barkov [1,*], Andrey A. Nikiforov [1], Robert F. Martin [2] and Vladimir N. Korolyuk [3]**

[1] Research Laboratory of Industrial and Ore Mineralogy, Cherepovets State University, 5 Lunacharsky Avenue, 162600 Cherepovets, Russia
[2] Department of Earth and Planetary Sciences, McGill University, 3450 University Street, Montreal, QC H3A 0E8, Canada
[3] V.S. Sobolev Institute of Geology and Mineralogy, Siberian Branch of the Russian Academy of Science, 3 Avenue "Prospekt Koptyuga", 630090 Novosibirsk, Russia
* Correspondence: ore-minerals@mail.ru

**Abstract:** For the first time, corona-type textures are described in ultrabasic rocks in three complexes of the Serpentinite Belt on the Kola Peninsula in the northeastern Fennoscandian Shield. Three variants of the corona texture formed at different stages during the crystallization of a komatiitic, Al-undepleted melt emplaced in a subvolcanic setting. The first type crystallized at an early stage (Mg# Ol = 87) in a fine-grained harzburgite of the Chapesvara-I sill, with the following order in the corona: Ol → Opx → Cpx → Pl → Amp (aluminous sodic-calcic). The second type displays the sequence Opx → Cpx → Amp → Pl → Qz, which is observed in the orthopyroxenite zone in the Lotmvara-I sill. The third type involves a symplectitic corona in a plagioclase-bearing orthopyroxenite in the Lyavaraka complex, in which the inferred order is: Cpx → Amp (aluminous hornblende) + symplectitic Qz, formed in direct contact with grains of Pl. The corona-type textures occur in fresh rocks and are not related to regional metamorphism. They likely formed as consequences of two important factors: (1) rapid cooling, leading to unsteady conditions of crystallization in a shallow setting; and (2) an intrinsic enrichment in $H_2O$ and other volatiles in the parental magma, giving rise to fluid-saturated environments at advanced stages of crystallization. This was followed by a deuteric deposition of Amp rims as a result of the accumulation of $H_2O$ and reaction of $H_2O$-bearing fluid with early grains of pyroxene and late plagioclase. The likely existence of a close relationship is suggested by the drusites of the Belomorian complex, which are coeval. In addition, unusual occurrences of lamellar inclusions of phlogopite and $Al_2SiO_5$ are documented, hosted by interstitial grains of plagioclase in the orthopyroxenite zone of the Lotmvara-I sill. These are attributed to crystallization from late portions of remaining melt enriched in Al, K, Na, $H_2O$, and Cl, which is indicated by the recorded occurrence of chlorapatite in this association. Thus, our findings indicate the presence and abundance of intrinsic volatiles, Cl, F, $CO_2$, and especially magmatic $H_2O$, which were important to lower the liquidus, decrease the density and viscosity of the highly magnesian melt of Al-undepleted komatiite, thus enabling its transport from the mantle to a shallow level in the crust.

**Keywords:** Chapesvara-I; Lotmvara-I; Lyavaraka; Serpentinite Belt; ultrabasic complexes; komatiite; corona textures; Kola Peninsula; Fennoscandian Shield



**Citation:** Barkov, A.Y.; Nikiforov, A.A.; Martin, R.F.; Korolyuk, V.N. Corona-Type Textures in Ultrabasic Complexes of the Serpentinite Belt, Kola Peninsula, Russia. *Minerals* **2023**, *13*, 115. https://doi.org/10.3390/min13010115

Received: 4 December 2022
Revised: 29 December 2022
Accepted: 5 January 2023
Published: 11 January 2023



## 1. Introduction

The corona texture commonly develops as a result of prograde or retrograde metamorphism [1]. However, it is also encountered in unmetamorphosed igneous rocks. In ultrabasic–basic rocks, concentric layers of one or several minerals cluster around an early phase developed in the core (normally olivine or orthopyroxene), commonly in close association with plagioclase. Indeed, the corona texture has been described in unmetamorphosed

subophitic olivine gabbro in the Black Hill complex, South Australia [2], and in ultrabasic–basic cumulates in the Genina Gharbia Alaskan-type complex, in the southeastern Desert of Egypt [3].

Our main aims are to describe the occurrence and discuss the significance of corona-type textures in three suites of ultrabasic compositions of the Serpentinite Belt in the Kola Peninsula in the Fennoscandian Shield. They were recorded in the orthopyroxenite zone of the Lotmvara-I sill, not described previously, as well as in the associated Chapesvara-I sill and the Lyavaraka complex. Along with a suite of smaller dislocated bodies of shallowly emplaced bodies of dunite–harzburgite–orthopyroxenite, these occurrences are strung out along the Serpentinite Belt–Tulppio Belt (or SB–TB megastructure) [4–7]. These complexes define a large igneous province of the Paleoproterozoic age, as inferred from the results of isotopic dating of the Pados-Tundra layered complex, 2485 ± 38 of Ma [8]. They are products of a large-scale mantle plume of rising komatiitic melt [4–7] that intruded in a within-plate setting [9,10]. They were emplaced in the interval 2.5–2.4 Ga with other members of the large igneous province of the Sumian cycle of igneous activity in the Fennoscandian Shield.

We describe the new occurrences of the corona texture to provide petrogenetic insight into features of the ultrabasic bodies of the northeastern Fennoscandian Shield. They point to the likely existence of a close relationship between the subvolcanic suites of the Serpentinite Belt (SB) and the so-called "drusites" of the Belomorian complex, which are coeval [11] with the SB. As described historically [12], drusites are corona-textured rocks of basic–ultrabasic composition [13], corresponding mostly to gabbronorite, that occur in the Karelia–Kola region of Russia [14,15]. We also describe a puzzling occurrence of micrometric lamellae of $Al_2SiO_5$ in a peraluminous assemblage encountered in the Lomtvara-I intrusive body. Our findings address the special conditions achieved at advanced stages of crystallization of these ultrabasic complexes.

## 2. Materials and Methods

### *2.1. Samples and Background Information*

Our study is based on a detailed examination of corona-textured samples of ultrabasic rocks collected from three complexes of the Serpentinite Belt in the Kola Peninsula: (1) The Lotmvara-I sill of the Lotmvara complex, (2) the Chapesvara-I sill of the Chapesvara complex, and (3) the Lyavaraka complex (Figure 1). The Lotmvara-I sill (Figures 2 and 3) as well as the neighboring Lotmvara-II suite (Barkov et al., unpubl. findings) may well represent shallow-level "crests" related to the deeper structures such as laccoliths or chonoliths. Details about the geological structures of the Chapesvara and Lyavaraka complexes (Figures 4 and 5) were previously provided [4,6].


**Figure 1.** Location of the investigated complexes in the Kola Peninsula, northwestern Russia. The Lotmvara-I sill is located about 20 km northwest of the Pados-Tundra intrusion (see Figures 2 and 3 for additional information).

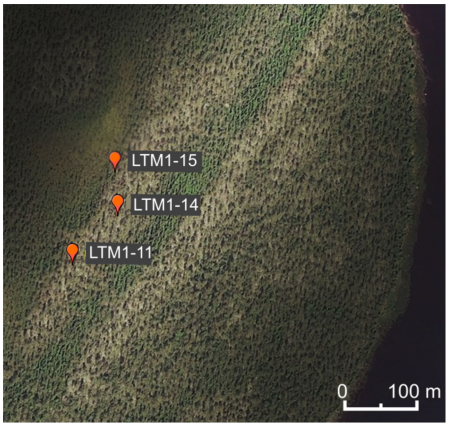


**Figure 2.** A satellite SAS.Planet image shows the sampling locations in three areas of the orthopyroxenite zone of the Lotmvara-I sill. The sill (N68°08′37.064″; E30°15′14.546″) is exposed largely along the two subparallel rows (gray) of northeastern strike, which are clearly visible on the image.

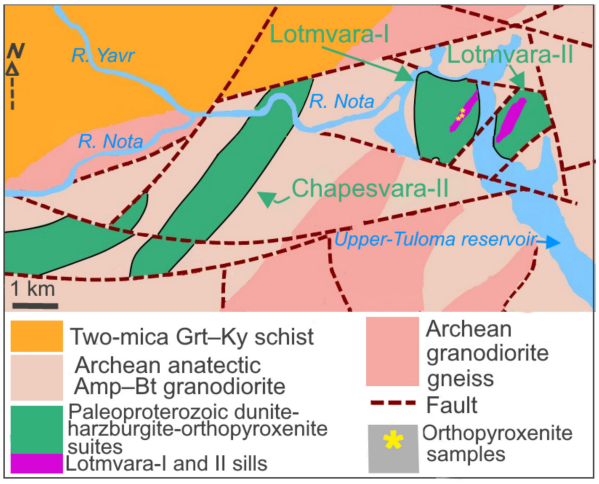


**Figure 3.** Schematic geological map shows the regional geology, modified slightly from [16], with the position of the sills of Lotmvara-I and II, which are based on the results of our mapping. The location of the sampling area is shown by a yellow star symbol, which corresponds to the orthopyroxenite zone of the Lotmvara-I sill.

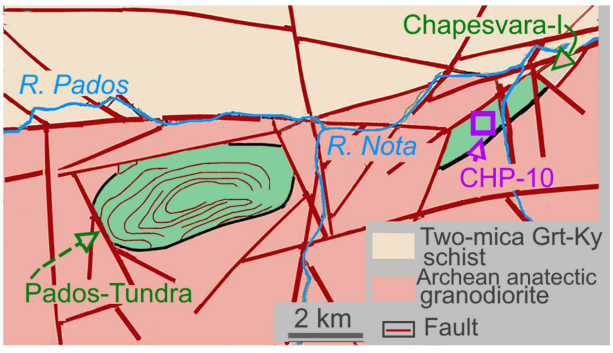


**Figure 4.** Schematic geological map shows the regional geology, modified slightly from [16]. The location of the sample CHP-10 is displayed by the purple square.

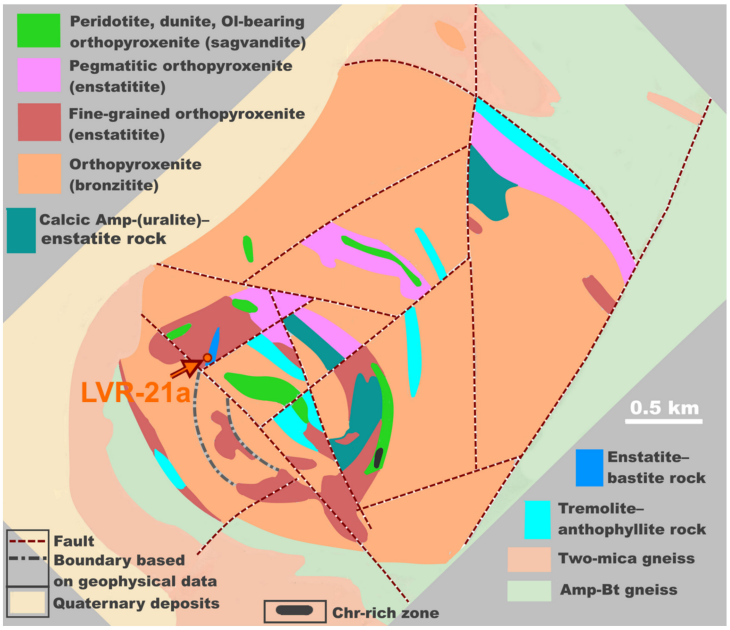


**Figure 5.** The location of the corona-textured sample (LVR-21a) is shown on a schematic geological map of the Lyavaraka complex, after Spirov [17].

### *2.2. Electron-Microprobe Analyses*

Representative specimens were analyzed at the Analytical Center for Multi-Elemental and Isotope Studies, SB RAS, Novosibirsk, Russia, using a JEOL JXA-8100 electron microprobe (produced by "Japan Electronics", Tokyo, Japan), operated in wavelength-dispersive spectrometry mode (WDS).

An accelerating voltage of 20 kV and a probe current of 30 to 50 nA were used. We employed the $K\alpha$ analytical lines for all elements except for Cr, where the $K\beta_1$ line was used instead because of peak overlap. The measurements were made on the peaks for 20 or 10 s. The superposition of the Ti$K\beta_1$ line on the V$K\alpha$ line and of the V$K\alpha$ line on the Cr$K\alpha$ line was accommodated using the OVERLAP CORRECTION software. The probe diameter was ~1–2 μm. Natural specimens of olivine (Mg, Si, Fe, and Ni) and chromiferous or manganiferous garnet (Ca, Cr, and Mn) were used as standards for olivine. Grains of orthopyroxene and hydrous silicates were analyzed using pyrope (Si, Al, and Fe), a glass Ti standard (GL-6), chromiferous garnet (Cr), diopside and pyrope (Mg and Ca), manganiferous garnet (Mn), albite (Na), and orthoclase (K). A natural specimen of magnesian chromite (for Cr, Fe, Mg, and Al), manganiferous garnet (Mn), ilmenite (Ti), and synthetic oxides $NiFe_2O_4$ (Ni), $ZnFe_2O_4$ (Zn), and $V_2O_5$ (V) were used as standards for chromian spinel. The calculated values of the detection limit (1σ criterion) are: ±0.01 wt.% for Ti, Cr, Fe, Ni, Ca, Zn, Mn, and K, and 0.02 wt.% (Na and Al). The minor and accessory minerals were analyzed at 20 kV and 30 to 50 nA using a finely focused beam (~2 μm) and using combinations of standard specimens of fluorapatite (F$K\alpha$), chlorapatite (Cl$K\alpha$), albite (Na$K\alpha$), Fe-bearing pyrope (Mg$K\alpha$, Fe$K\alpha$), diopside (Ca$K\alpha$), orthoclase (K$K\alpha$, Al$K\alpha$, Si$K\alpha$), kyanite (Al$K\alpha$, Si$K\alpha$), manganiferous garnet (Mn$K\alpha$), synthetic phosphates ($CePO_4$, $LaPO_4$, $YPO_4$, among others), zircon (REE$L\alpha$; Zr$L\alpha$), $BaSiO_3$ (Ba$L\alpha$), $SrSiO_3$ (Sr$L\alpha$), and Ti-bearing chromite (Cr$K\alpha$ and Ti$K\alpha$). The ZAF or Phi-Rho-Z procedures were used; the Ti–Ba peak overlaps were corrected. Other details of the analytical procedures were described previously [18].

## 3. Results and Observations

### *3.1. Corona-Type Texture in the Lotmvara-I Sill*

The exposed portions of the sill represent chains of blocks (up to 5–8 m across); in addition, flat surfaces of bedrock outcrops are observed locally. The specimens of orthopyroxenite that were examined in three areas of the sill (Figure 1) were all similar

(Figure 6a–c). They were fairly fresh, unfoliated, and composed dominantly of well-formed crystals of green-colored orthopyroxene ($Wo_{2.8–3.6}En_{79.6–83.1}Fs_{13.8–17.0}Aeg_{0–0.4}$; Mg# 79.2–83.5) that seem to be adcumulates (Figure 7). Occurrences of interstitial plagioclase ($An_{41.9–54.9}Ab_{45.0–57.7}Or_{0.2–0.4}$) are minor and are associated with grains of calcic amphibole of tremolite composition (Figure 7). Accessory minerals are represented by grains of chromian spinel (Mg# 22.0–26.4) and Cr-bearing rutile (or its polymorph), with 0.84–0.97 wt.% $Cr_2O_3$. Detailed results of electron-microprobe analyses are reported in Tables 1–4. Green-colored Opx is typical of complexes of the Serpentinite Belt, including the Pados-Tundra layered complex. In outcrops, the specimens shown here display a grayish or brownish tint.


**Figure 6.** *Cont.*


**Figure 6.** (**a**–**e**). Specimens of orthopyroxenite from the Lotmvara-I and Lyavaraka complexes (Figure 6a–c,e, respectively) and of fine-grained to microgranular harzburgite from the Chapesvara-I complex (Figure 6d).

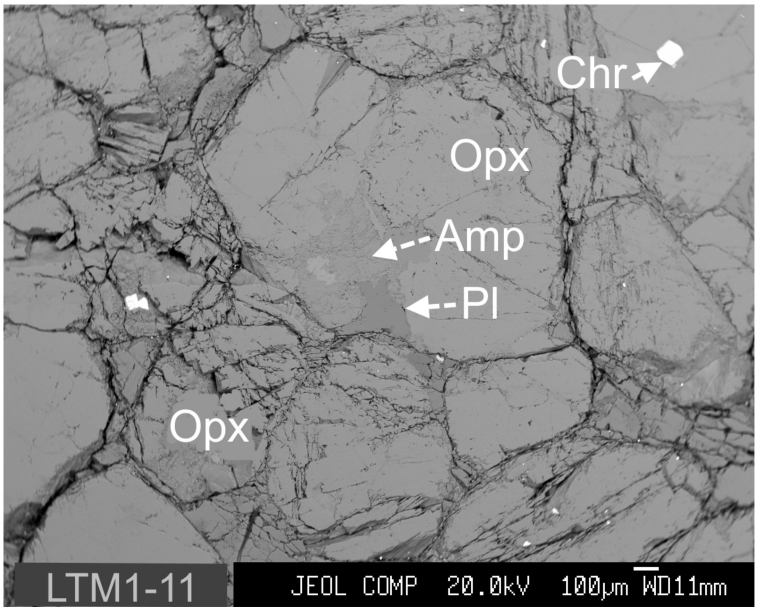


**Figure 7.** A back-scattered electron image (BSE) displays a specimen of orthopyroxenite (Figure 6a) composed mostly of grains of orthopyroxene (Opx) with the presence of minor quantities of amphibole (Amp) and plagioclase (Pl). The location of this sample, Ltm1-11, is shown in Figure 1.

**Table 1.** Compositions of pyroxenes in the orthopyroxenite zone of the Lotmvara-I sill, Kola Peninsula.

| # | Sample | $SiO_2$ | $TiO_2$ | $Al_2O_3$ | $Cr_2O_3$ | FeO | MnO | MgO | CaO | $Na_2O$ | $K_2O$ | Total |
|---|---|---|---|---|---|---|---|---|---|---|---|---|
| 1 | LTM1-11 Opx1 1 | 56.54 | 0.05 | 1.29 | 0.56 | 9.22 | 0.22 | 30.61 | 1.61 | 0.06 | 0.01 | 100.15 |
| 2 | LTM1-11 Opx1 2 | 56.44 | 0.04 | 1.26 | 0.57 | 9.14 | 0.19 | 29.98 | 1.59 | 0.04 | n.d. | 99.24 |
| 3 | LTM1-11 Opx2 1 | 56.21 | 0.06 | 1.45 | 0.64 | 8.99 | 0.19 | 30.58 | 1.60 | 0.09 | n.d. | 99.81 |

**Table 1.** *Cont.*

| # | Sample | $SiO_2$ | $TiO_2$ | $Al_2O_3$ | $Cr_2O_3$ | FeO | MnO | MgO | CaO | $Na_2O$ | $K_2O$ | Total |
|---|---|---|---|---|---|---|---|---|---|---|---|---|
| 4 | LTM1-11 Opx2 2 | 56.89 | 0.02 | 1.39 | 0.60 | 9.02 | 0.18 | 30.39 | 1.54 | 0.07 | 0.01 | 100.09 |
| 5 | LTM1-11 Opx3 1 | 56.78 | 0.10 | 1.32 | 0.59 | 8.90 | 0.18 | 30.78 | 1.45 | 0.02 | 0.01 | 100.13 |
| 6 | LTM1-11 Opx3 2 | 56.88 | 0.10 | 1.17 | 0.57 | 8.79 | 0.17 | 30.66 | 1.43 | 0.04 | n.d. | 99.81 |
| 7 | LTM1-14 Opx1 1 | 55.99 | 0.06 | 1.37 | 0.61 | 10.72 | 0.23 | 28.91 | 1.52 | 0.04 | 0.01 | 99.46 |
| 8 | LTM1-14 Opx1 2 | 56.30 | 0.06 | 1.37 | 0.64 | 10.51 | 0.18 | 28.78 | 1.76 | 0.07 | n.d. | 99.65 |
| 9 | LTM1-14 Opx2 1 | 56.40 | 0.05 | 1.50 | 0.63 | 10.32 | 0.22 | 28.95 | 1.79 | n.d. | n.d. | 99.87 |
| 10 | LTM1-14 Opx2 2 | 55.77 | 0.06 | 1.57 | 0.69 | 10.44 | 0.23 | 28.76 | 1.80 | 0.08 | n.d. | 99.39 |
| 11 | LTM1-14 Opx3 1 | 56.29 | 0.13 | 1.40 | 0.68 | 9.96 | 0.19 | 29.50 | 1.65 | 0.05 | n.d. | 99.85 |
| 12 | LTM1-14 Opx3 2 | 56.25 | 0.07 | 1.41 | 0.70 | 10.01 | 0.17 | 29.29 | 1.41 | 0.09 | n.d. | 99.38 |
| 13 | LTM1-14 Opx4 1 | 56.24 | 0.08 | 1.19 | 0.62 | 8.94 | 0.17 | 30.49 | 1.47 | 0.01 | 0.01 | 99.20 |
| 14 | LTM1-14 Opx4 2 | 56.58 | 0.05 | 1.20 | 0.64 | 8.93 | 0.20 | 30.65 | 1.45 | 0.09 | n.d. | 99.79 |
| 15 | LTM1-14 Opx5 1 | 56.54 | 0.06 | 1.34 | 0.68 | 8.76 | 0.19 | 30.18 | 1.51 | 0.05 | 0.01 | 99.31 |
| 16 | LTM1-14 Opx5 2 | 56.73 | 0.06 | 1.36 | 0.74 | 8.82 | 0.18 | 30.36 | 1.51 | 0.09 | 0.01 | 99.85 |
| 17 | LTM1-14 Opx6 1 | 56.64 | 0.06 | 1.39 | 0.76 | 8.78 | 0.19 | 29.72 | 1.52 | 0.07 | n.d. | 99.12 |
| 18 | LTM1-14 Opx6 2 | 56.67 | 0.06 | 1.37 | 0.76 | 8.77 | 0.18 | 29.87 | 1.66 | 0.11 | 0.01 | 99.47 |
| 19 | LTM1-15 Opx1 1 | 55.70 | 0.06 | 1.39 | 0.61 | 9.11 | 0.21 | 30.48 | 1.60 | 0.04 | 0.01 | 99.20 |
| 20 | LTM1-15 Opx1 2 | 55.08 | 0.32 | 1.39 | 0.61 | 9.14 | 0.21 | 30.64 | 1.68 | 0.09 | n.d. | 99.17 |
| 21 | LTM1-15 Opx2 1 | 55.59 | 0.24 | 1.35 | 0.57 | 9.26 | 0.20 | 31.00 | 1.38 | 0.05 | n.d. | 99.64 |
| 22 | LTM1-15 Opx2 2 | 55.53 | 0.09 | 1.43 | 0.59 | 9.18 | 0.23 | 30.79 | 1.53 | 0.00 | n.d. | 99.37 |
| 23 | LTM1-15 Opx2 3 | 55.82 | 0.06 | 1.46 | 0.60 | 9.18 | 0.20 | 30.86 | 1.52 | 0.09 | 0.01 | 99.79 |
| 24 | LTM1-15 Opx3 1 | 55.82 | 0.09 | 1.40 | 0.59 | 9.03 | 0.21 | 31.26 | 1.28 | 0.02 | n.d. | 99.71 |
| 25 | LTM1-15 Opx3 2 | 55.98 | 0.05 | 1.27 | 0.58 | 8.92 | 0.19 | 31.08 | 1.53 | 0.03 | 0.01 | 99.64 |
| 26 | LTM1-14 Cpx1 1 | 53.39 | 0.25 | 3.03 | 1.08 | 6.66 | 0.18 | 17.57 | 17.47 | 0.37 | 0.02 | 100.00 |
| 27 | LTM1-14 Cpx1 2 | 53.05 | 0.22 | 3.18 | 1.06 | 6.70 | 0.15 | 17.78 | 17.00 | 0.30 | 0.01 | 99.44 |
| 28 | LTM1-14 Cpx2 1 | 53.15 | 0.37 | 3.03 | 1.04 | 5.91 | 0.16 | 16.77 | 19.18 | 0.51 | n.d. | 100.10 |
| 29 | LTM1-14 Cpx2 2 | 52.71 | 0.38 | 3.27 | 1.13 | 5.13 | 0.16 | 15.70 | 20.21 | 0.56 | n.d. | 99.24 |
| 30 | LTM1-14 Cpx3 1 | 53.18 | 0.29 | 2.84 | 1.08 | 3.74 | 0.12 | 15.29 | 22.27 | 0.54 | n.d. | 99.35 |
| 31 | LTM1-14 Cpx3 2 | 53.46 | 0.23 | 2.65 | 1.12 | 6.02 | 0.17 | 17.54 | 17.70 | 0.49 | n.d. | 99.38 |

***apfu***

| | Si | Ti | Al | Cr | Fe | Mn | Mg | Ca | Na | K | Wo | En | Fs | Aeg | Mg# |
|---|---|---|---|---|---|---|---|---|---|---|---|---|---|---|---|
| 1 | 1.99 | 0.001 | 0.05 | 0.02 | 0.27 | 0.006 | 1.60 | 0.06 | 0.004 | 0.000 | 3.1 | 82.4 | 14.3 | 0.2 | 83.6 |
| 2 | 2.00 | 0.001 | 0.05 | 0.02 | 0.27 | 0.006 | 1.59 | 0.06 | 0.002 | 0.000 | 3.1 | 82.4 | 14.4 | 0.1 | 81.8 |
| 3 | 1.98 | 0.002 | 0.06 | 0.02 | 0.26 | 0.006 | 1.60 | 0.06 | 0.006 | 0.000 | 3.1 | 82.7 | 13.9 | 0.3 | 84.1 |
| 4 | 2.00 | 0.000 | 0.06 | 0.02 | 0.26 | 0.005 | 1.59 | 0.06 | 0.005 | 0.000 | 3.0 | 82.7 | 14.0 | 0.3 | 82.4 |
| 5 | 1.99 | 0.003 | 0.05 | 0.02 | 0.26 | 0.005 | 1.61 | 0.05 | 0.001 | 0.000 | 2.8 | 83.3 | 13.8 | 0.1 | 83.1 |
| 6 | 2.00 | 0.003 | 0.05 | 0.02 | 0.26 | 0.005 | 1.61 | 0.05 | 0.003 | 0.000 | 2.8 | 83.4 | 13.7 | 0.1 | 82.7 |
| 7 | 2.00 | 0.002 | 0.06 | 0.02 | 0.32 | 0.007 | 1.54 | 0.06 | 0.003 | 0.000 | 3.0 | 79.8 | 17.0 | 0.1 | 79.5 |
| 8 | 2.00 | 0.001 | 0.06 | 0.02 | 0.31 | 0.006 | 1.53 | 0.07 | 0.005 | 0.000 | 3.5 | 79.7 | 16.6 | 0.2 | 79.2 |
| 9 | 2.00 | 0.001 | 0.06 | 0.02 | 0.31 | 0.007 | 1.53 | 0.07 | 0.000 | 0.000 | 3.6 | 80.1 | 16.4 | 0.0 | 79.2 |
| 10 | 1.99 | 0.002 | 0.07 | 0.02 | 0.31 | 0.007 | 1.53 | 0.07 | 0.006 | 0.000 | 3.6 | 79.6 | 16.6 | 0.3 | 80.0 |
| 11 | 1.99 | 0.003 | 0.06 | 0.02 | 0.30 | 0.006 | 1.56 | 0.06 | 0.003 | 0.000 | 3.3 | 80.9 | 15.6 | 0.2 | 80.8 |
| 12 | 2.00 | 0.002 | 0.06 | 0.02 | 0.30 | 0.005 | 1.55 | 0.05 | 0.006 | 0.000 | 2.8 | 81.1 | 15.8 | 0.3 | 80.2 |
| 13 | 1.99 | 0.002 | 0.05 | 0.02 | 0.26 | 0.005 | 1.61 | 0.06 | 0.000 | 0.000 | 2.9 | 83.1 | 13.9 | 0.0 | 83.1 |
| 14 | 1.99 | 0.001 | 0.05 | 0.02 | 0.26 | 0.006 | 1.61 | 0.05 | 0.006 | 0.000 | 2.8 | 83.0 | 13.9 | 0.3 | 83.5 |
| 15 | 2.00 | 0.002 | 0.06 | 0.02 | 0.26 | 0.006 | 1.59 | 0.06 | 0.004 | 0.000 | 3.0 | 83.0 | 13.8 | 0.2 | 82.2 |
| 16 | 2.00 | 0.002 | 0.06 | 0.02 | 0.26 | 0.005 | 1.59 | 0.06 | 0.006 | 0.000 | 3.0 | 82.9 | 13.8 | 0.3 | 82.6 |
| 17 | 2.01 | 0.001 | 0.06 | 0.02 | 0.26 | 0.006 | 1.58 | 0.06 | 0.005 | 0.000 | 3.0 | 82.7 | 14.0 | 0.2 | 80.9 |
| 18 | 2.01 | 0.002 | 0.06 | 0.02 | 0.26 | 0.005 | 1.58 | 0.06 | 0.007 | 0.000 | 3.3 | 82.4 | 13.9 | 0.4 | 81.7 |
| 19 | 1.97 | 0.001 | 0.06 | 0.02 | 0.27 | 0.006 | 1.61 | 0.06 | 0.003 | 0.001 | 3.1 | 82.6 | 14.1 | 0.1 | 84.4 |
| 20 | 1.95 | 0.008 | 0.06 | 0.02 | 0.27 | 0.006 | 1.62 | 0.06 | 0.006 | 0.000 | 3.2 | 82.3 | 14.1 | 0.3 | 85.9 |
| 21 | 1.96 | 0.006 | 0.06 | 0.02 | 0.27 | 0.006 | 1.63 | 0.05 | 0.003 | 0.000 | 2.7 | 83.0 | 14.2 | 0.2 | 85.4 |
| 22 | 1.96 | 0.002 | 0.06 | 0.02 | 0.27 | 0.007 | 1.62 | 0.06 | 0.000 | 0.000 | 3.0 | 82.8 | 14.2 | 0.0 | 85.1 |
| 23 | 1.96 | 0.002 | 0.06 | 0.02 | 0.27 | 0.006 | 1.62 | 0.06 | 0.006 | 0.000 | 2.9 | 82.6 | 14.1 | 0.3 | 85.4 |
| 24 | 1.96 | 0.002 | 0.06 | 0.02 | 0.27 | 0.006 | 1.64 | 0.05 | 0.002 | 0.000 | 2.5 | 83.6 | 13.9 | 0.1 | 85.6 |
| 25 | 1.97 | 0.001 | 0.05 | 0.02 | 0.26 | 0.006 | 1.63 | 0.06 | 0.002 | 0.000 | 3.0 | 83.3 | 13.7 | 0.1 | 85.4 |
| 26 | 1.95 | 0.007 | 0.13 | 0.03 | 0.20 | 0.006 | 0.96 | 0.68 | 0.026 | 0.001 | 36.4 | 51.0 | 11.1 | 1.4 | 78.4 |
| 27 | 1.95 | 0.006 | 0.14 | 0.03 | 0.21 | 0.005 | 0.97 | 0.67 | 0.021 | 0.000 | 35.7 | 51.9 | 11.2 | 1.1 | 78.4 |

**Table 1.** *Cont.*

| # | Sample | | $SiO_2$ | $TiO_2$ | $Al_2O_3$ | $Cr_2O_3$ | FeO | MnO | MgO | CaO | | $Na_2O$ | $K_2O$ | Total |
|---|---|---|---|---|---|---|---|---|---|---|---|---|---|---|
| 28 | 1.94 | 0.010 | 0.13 | 0.03 | 0.18 | 0.005 | 0.91 | 0.75 | 0.036 | 0.000 | 39.8 | 48.4 | 9.8 | 1.9 | 80.9 |
| 29 | 1.95 | 0.011 | 0.14 | 0.03 | 0.16 | 0.005 | 0.86 | 0.80 | 0.040 | 0.000 | 42.8 | 46.3 | 8.8 | 2.1 | 80.2 |
| 30 | 1.96 | 0.008 | 0.12 | 0.03 | 0.12 | 0.004 | 0.84 | 0.88 | 0.038 | 0.000 | 46.9 | 44.8 | 6.3 | 2.0 | 83.0 |
| 31 | 1.96 | 0.006 | 0.11 | 0.03 | 0.18 | 0.005 | 0.96 | 0.70 | 0.035 | 0.000 | 37.0 | 51.0 | 10.1 | 1.9 | 79.8 |

Note. Results of electron-microprobe analyses conducted by wavelength-dispersive spectrometry are listed in weight %. n.d.: not detected (below detection limits). Apfu: atoms per formula unit based on six oxygen atoms. Wo: wollastonite; En: enstatite; Fs: ferrosilite; Aeg: aegirine; Opx is orthopyroxene; Cpx is clinopyroxene. Mg# = 100Mg/(Mg + $Fe^{2+}$ + Mn).

**Table 2.** Compositions of amphiboles in the orthopyroxenite zone of the Lotmvara-I sill, Kola Peninsula.

| # | Sample | $SiO_2$ | $TiO_2$ | $Al_2O_3$ | $Cr_2O_3$ | FeO | MnO | MgO | CaO | $Na_2O$ | $K_2O$ | Total |
|---|---|---|---|---|---|---|---|---|---|---|---|---|
| 1 | LTM1-11 Tr1 1 | 56.30 | 0.15 | 2.99 | 0.77 | 3.06 | 0.08 | 21.18 | 11.68 | 0.47 | 0.05 | 96.73 |
| 2 | LTM1-11 Tr1 2 | 55.78 | 0.14 | 3.06 | 0.85 | 3.11 | 0.11 | 20.50 | 11.83 | 0.54 | 0.04 | 97.96 |
| 3 | LTM1-11 Tr2 1 | 56.22 | 0.15 | 2.92 | 0.84 | 3.03 | 0.10 | 20.84 | 11.68 | 0.53 | 0.05 | 98.36 |
| 4 | LTM1-11 Tr2 2 | 56.32 | 0.11 | 2.78 | 0.81 | 3.00 | 0.08 | 20.58 | 11.57 | 0.56 | 0.05 | 97.86 |
| 5 | LTM1-11 Tr3 | 56.46 | 1.59 | 3.22 | 1.23 | 3.42 | 0.08 | 20.29 | 12.00 | 0.44 | 0.06 | 100.79 |
| 6 | LTM1-14 Tr1 1 | 55.94 | 0.38 | 2.72 | 0.82 | 3.76 | 0.07 | 20.41 | 12.53 | 0.30 | 0.04 | 98.97 |
| 7 | LTM1-14 Tr1 2 | 56.26 | 0.26 | 2.60 | 0.82 | 3.73 | 0.10 | 20.68 | 12.52 | 0.32 | 0.05 | 99.34 |
| 8 | LTM1-14 Tr2 1 | 55.91 | 0.28 | 3.12 | 0.90 | 3.83 | 0.07 | 20.11 | 12.58 | 0.32 | 0.03 | 99.15 |
| 9 | LTM1-14 Tr2 2 | 55.65 | 0.24 | 3.13 | 0.91 | 3.86 | 0.08 | 20.02 | 12.51 | 0.36 | 0.05 | 98.81 |
| 10 | LTM1-14 Tr3 1 | 55.36 | 0.66 | 3.02 | 0.84 | 3.79 | 0.08 | 20.33 | 12.39 | 0.42 | 0.04 | 98.93 |
| 11 | LTM1-14 Tr3 2 | 55.58 | 0.16 | 3.23 | 0.84 | 3.83 | 0.10 | 20.49 | 12.48 | 0.38 | 0.05 | 99.14 |
| 12 | LTM1-14 Tr3 3 | 56.07 | 0.17 | 2.98 | 0.79 | 3.77 | 0.07 | 20.30 | 12.34 | 0.39 | 0.03 | 98.91 |
| 13 | LTM1-14 Tr3 4 | 55.26 | 0.41 | 3.90 | 1.00 | 3.95 | 0.07 | 20.16 | 12.30 | 0.47 | 0.05 | 99.57 |
| 14 | LTM1-14 Tr4 1 | 56.82 | 0.11 | 2.05 | 0.49 | 3.50 | 0.09 | 21.25 | 12.51 | 0.33 | 0.04 | 99.19 |
| 15 | LTM1-14 Tr4 2 | 56.89 | 0.10 | 2.18 | 0.54 | 3.53 | 0.10 | 21.17 | 12.49 | 0.30 | 0.06 | 99.36 |
| 16 | LTM1-14 Tr4 3 | 57.34 | 0.08 | 1.62 | 0.52 | 3.21 | 0.10 | 21.48 | 12.49 | 0.19 | 0.03 | 99.06 |
| 17 | LTM1-14 Tr4 4 | 55.62 | 0.17 | 2.68 | 1.05 | 3.77 | 0.08 | 20.39 | 12.37 | 0.39 | 0.05 | 98.57 |
| 18 | LTM1-14 Tr5 5 | 56.23 | 0.29 | 2.32 | 0.76 | 3.49 | 0.08 | 21.05 | 12.76 | 0.26 | 0.04 | 99.28 |
| 19 | LTM1-14 Tr5 1 | 56.62 | 0.26 | 2.30 | 0.74 | 3.31 | 0.07 | 21.22 | 12.10 | 0.32 | 0.05 | 98.99 |
| 20 | LTM1-14 Tr5 2 | 56.32 | 0.30 | 2.24 | 0.72 | 3.36 | 0.09 | 21.16 | 12.19 | 0.38 | 0.03 | 98.79 |
| 21 | LTM1-14 Tr5 3 | 56.18 | 0.19 | 2.71 | 0.77 | 3.44 | 0.08 | 21.15 | 12.16 | 0.41 | 0.05 | 99.14 |
| 22 | LTM1-14 Tr5 4 | 56.01 | 0.12 | 2.58 | 0.99 | 3.61 | 0.08 | 21.08 | 12.07 | 0.40 | 0.06 | 99.00 |
| 23 | LTM1-15 Ath1 1 | 56.07 | 0.05 | 2.49 | 0.93 | 8.85 | 0.24 | 26.18 | 2.40 | 0.40 | 0.02 | 99.63 |
| 24 | LTM1-15 Ath1 2 | 56.55 | 0.07 | 2.66 | 0.52 | 8.59 | 0.20 | 26.17 | 2.42 | 0.46 | 0.03 | 99.67 |
| 25 | LTM1-15 Ath2 1 | 58.30 | 0.03 | 0.94 | 0.16 | 9.11 | 0.22 | 28.00 | 0.76 | 0.16 | 0.01 | 99.69 |
| 26 | LTM1-15 Ath2 2 | 58.08 | 0.05 | 1.14 | 0.21 | 8.83 | 0.24 | 27.79 | 0.69 | 0.21 | 0.04 | 99.28 |

***apfu***

| # | Si | Ti | Al | Cr | $Fe^{3+}$ | $Fe^{2+}$ | $Mn^{2+}$ | Mg | Ca | Na | K | OH (calc.) | Mg# |
|---|---|---|---|---|---|---|---|---|---|---|---|---|---|
| 1 | 7.73 | 0.02 | 0.48 | 0.08 | 0.00 | 0.35 | 0.01 | 4.33 | 1.72 | 0.13 | 0.01 | 1.83 | 92.3 |
| 2 | 7.76 | 0.02 | 0.50 | 0.09 | 0.17 | 0.19 | 0.01 | 4.25 | 1.76 | 0.15 | 0.01 | 1.86 | 95.5 |
| 3 | 7.77 | 0.02 | 0.48 | 0.09 | 0.27 | 0.09 | 0.01 | 4.29 | 1.73 | 0.14 | 0.01 | 1.84 | 97.7 |
| 4 | 7.82 | 0.01 | 0.46 | 0.09 | 0.18 | 0.17 | 0.01 | 4.26 | 1.72 | 0.15 | 0.01 | 1.86 | 95.9 |
| 5 | 7.68 | 0.16 | 0.52 | 0.13 | 0.05 | 0.34 | 0.01 | 4.11 | 1.75 | 0.12 | 0.01 | 1.82 | 92.2 |
| 6 | 7.76 | 0.04 | 0.45 | 0.09 | 0.05 | 0.38 | 0.01 | 4.22 | 1.86 | 0.08 | 0.01 | 1.85 | 91.5 |
| 7 | 7.76 | 0.03 | 0.42 | 0.09 | 0.11 | 0.32 | 0.01 | 4.25 | 1.85 | 0.09 | 0.01 | 1.84 | 92.8 |
| 8 | 7.75 | 0.03 | 0.51 | 0.10 | 0.00 | 0.44 | 0.01 | 4.16 | 1.87 | 0.09 | 0.01 | 1.85 | 90.2 |
| 9 | 7.75 | 0.03 | 0.51 | 0.10 | 0.00 | 0.45 | 0.01 | 4.16 | 1.87 | 0.10 | 0.01 | 1.86 | 90.0 |
| 10 | 7.69 | 0.07 | 0.49 | 0.09 | 0.10 | 0.35 | 0.01 | 4.21 | 1.84 | 0.11 | 0.01 | 1.85 | 92.1 |
| 11 | 7.69 | 0.02 | 0.53 | 0.09 | 0.17 | 0.28 | 0.01 | 4.22 | 1.85 | 0.10 | 0.01 | 1.85 | 93.6 |
| 12 | 7.77 | 0.02 | 0.49 | 0.09 | 0.08 | 0.36 | 0.01 | 4.19 | 1.83 | 0.11 | 0.01 | 1.85 | 91.9 |
| 13 | 7.61 | 0.04 | 0.63 | 0.11 | 0.18 | 0.27 | 0.01 | 4.14 | 1.82 | 0.13 | 0.01 | 1.84 | 93.7 |
| 14 | 7.83 | 0.01 | 0.33 | 0.05 | 0.15 | 0.25 | 0.01 | 4.36 | 1.85 | 0.09 | 0.01 | 1.84 | 94.4 |

**Table 2.** *Cont.*

| # | Sample | | $SiO_2$ | $TiO_2$ | $Al_2O_3$ | $Cr_2O_3$ | FeO | MnO | MgO | CaO | $Na_2O$ | $K_2O$ | Total |
|---|---|---|---|---|---|---|---|---|---|---|---|---|---|
| 15 | 7.82 | 0.01 | 0.35 | 0.06 | 0.16 | 0.25 | 0.01 | 4.34 | 1.84 | 0.08 | 0.01 | 1.84 | 94.3 |
| 16 | 7.89 | 0.01 | 0.26 | 0.06 | 0.15 | 0.22 | 0.01 | 4.41 | 1.84 | 0.05 | 0.01 | 1.84 | 95.0 |
| 17 | 7.75 | 0.02 | 0.44 | 0.12 | 0.11 | 0.33 | 0.01 | 4.23 | 1.85 | 0.11 | 0.01 | 1.86 | 92.6 |
| 18 | 7.76 | 0.03 | 0.38 | 0.08 | 0.10 | 0.30 | 0.01 | 4.33 | 1.89 | 0.07 | 0.01 | 1.84 | 93.3 |
| 19 | 7.78 | 0.03 | 0.37 | 0.08 | 0.27 | 0.11 | 0.01 | 4.35 | 1.78 | 0.09 | 0.01 | 1.84 | 97.3 |
| 20 | 7.77 | 0.03 | 0.36 | 0.08 | 0.24 | 0.15 | 0.01 | 4.35 | 1.80 | 0.10 | 0.01 | 1.84 | 96.5 |
| 21 | 7.72 | 0.02 | 0.44 | 0.08 | 0.30 | 0.10 | 0.01 | 4.33 | 1.79 | 0.11 | 0.01 | 1.84 | 97.5 |
| 22 | 7.71 | 0.01 | 0.42 | 0.11 | 0.35 | 0.07 | 0.01 | 4.33 | 1.78 | 0.11 | 0.01 | 1.84 | 98.2 |
| 23 | 7.72 | 0.01 | 0.40 | 0.10 | 0.00 | 1.02 | 0.03 | 5.37 | 0.35 | 0.11 | 0.00 | 1.84 | 83.6 |
| 24 | 7.77 | 0.01 | 0.43 | 0.06 | 0.00 | 0.99 | 0.02 | 5.36 | 0.36 | 0.12 | 0.01 | 1.84 | 84.1 |
| 25 | 7.96 | 0.00 | 0.15 | 0.02 | 0.00 | 1.04 | 0.03 | 5.70 | 0.11 | 0.04 | 0.00 | 1.82 | 84.2 |
| 26 | 7.97 | 0.01 | 0.18 | 0.02 | 0.00 | 1.01 | 0.03 | 5.68 | 0.10 | 0.06 | 0.01 | 1.83 | 84.5 |

Note. Results of electron-microprobe analyses conducted by wavelength-dispersive spectrometry are listed in weight %. Apfu: atoms per formula unit based on 23 oxygen atoms. Tr: tremolite; Ath: anthophyllite. Mg# = 100Mg/(Mg + $Fe^{2+}$ + Mn).

**Table 3.** Compositions of plagioclase in the orthopyroxenite zone of the Lotmvara-I sill, Kola Peninsula.

| # | Sample | $SiO_2$ | $TiO_2$ | $Al_2O_3$ | FeO | CaO | $Na_2O$ | $K_2O$ | Total (wt.%) | Si (apfu) | Al | Ca | Na | K | Or | Ab | An |
|---|---|---|---|---|---|---|---|---|---|---|---|---|---|---|---|---|---|
| 1 | LTM1-11 Pl1 1 | 59.38 | 0.01 | 25.67 | 0.04 | 7.60 | 6.91 | 0.02 | 99.62 | 2.65 | 1.35 | 0.36 | 0.60 | 0.00 | 0.1 | 62.1 | 37.8 |
| 2 | LTM1-11 Pl1 2 | 59.21 | n.d. | 25.74 | 0.05 | 7.70 | 7.00 | 0.02 | 99.72 | 2.65 | 1.36 | 0.37 | 0.61 | 0.00 | 0.1 | 62.1 | 37.8 |
| 3 | LTM1-11 Pl2 1 | 62.87 | 0.07 | 23.41 | 0.10 | 5.25 | 7.89 | 0.08 | 99.68 | 2.78 | 1.22 | 0.25 | 0.68 | 0.00 | 0.5 | 72.7 | 26.8 |
| 4 | LTM1-11 Pl2 2 | 61.29 | 0.08 | 24.17 | 0.10 | 5.75 | 7.48 | 0.06 | 98.92 | 2.74 | 1.27 | 0.28 | 0.65 | 0.00 | 0.4 | 69.9 | 29.7 |
| 5 | LTM1-11 Pl3 1 | 57.70 | 0.02 | 26.19 | 0.20 | 8.22 | 6.76 | 0.24 | 99.32 | 2.60 | 1.39 | 0.40 | 0.59 | 0.01 | 1.4 | 59.0 | 39.7 |
| 6 | LTM1-11 Pl3 2 | 58.79 | n.d. | 25.43 | 0.13 | 8.04 | 7.30 | 0.03 | 99.72 | 2.64 | 1.34 | 0.39 | 0.63 | 0.00 | 0.2 | 62.1 | 37.8 |
| 7 | LTM1-11 Pl4 1 | 55.49 | 0.11 | 28.21 | 0.03 | 10.65 | 5.23 | 0.06 | 99.79 | 2.50 | 1.50 | 0.51 | 0.46 | 0.00 | 0.3 | 46.9 | 52.7 |
| 8 | LTM1-11 Pl4 2 | 55.53 | 0.07 | 28.28 | 0.03 | 10.73 | 5.41 | 0.04 | 100.09 | 2.50 | 1.50 | 0.52 | 0.47 | 0.00 | 0.2 | 47.6 | 52.2 |
| 9 | LTM1-11 Pl 5 | 60.38 | 0.03 | 24.95 | 0.07 | 7.08 | 7.52 | 0.06 | 100.09 | 2.69 | 1.31 | 0.34 | 0.65 | 0.00 | 0.3 | 65.6 | 34.1 |
| 10 | LTM1-14 Pl1 1 | 58.12 | 0.08 | 26.44 | 0.05 | 8.31 | 6.33 | 0.06 | 99.38 | 2.61 | 1.40 | 0.40 | 0.55 | 0.00 | 0.3 | 57.7 | 41.9 |
| 11 | LTM1-14 Pl1 2 | 58.27 | 0.11 | 26.51 | 0.03 | 8.42 | 6.35 | 0.05 | 99.75 | 2.61 | 1.40 | 0.40 | 0.55 | 0.00 | 0.3 | 57.5 | 42.1 |
| 12 | LTM1-14 Pl2 1 | 56.14 | 0.17 | 27.68 | 0.07 | 9.84 | 5.56 | 0.05 | 99.51 | 2.53 | 1.47 | 0.47 | 0.49 | 0.00 | 0.3 | 50.4 | 49.3 |
| 13 | LTM1-14 Pl2 2 | 56.02 | 0.09 | 27.76 | 0.09 | 10.00 | 5.65 | 0.04 | 99.64 | 2.52 | 1.47 | 0.48 | 0.49 | 0.00 | 0.2 | 50.4 | 49.4 |
| 14 | LTM1-14 Pl3 1 | 55.75 | 0.09 | 27.85 | 0.07 | 10.00 | 5.52 | 0.04 | 99.32 | 2.52 | 1.48 | 0.48 | 0.48 | 0.00 | 0.2 | 49.9 | 49.9 |
| 15 | LTM1-14 Pl3 2 | 55.20 | 0.07 | 28.07 | 0.09 | 10.31 | 5.28 | 0.06 | 99.08 | 2.50 | 1.50 | 0.50 | 0.46 | 0.00 | 0.4 | 47.9 | 51.7 |
| 16 | LTM1-14 Pl3 3 | 54.44 | 0.03 | 28.73 | 0.07 | 11.12 | 5.03 | 0.03 | 99.44 | 2.47 | 1.53 | 0.54 | 0.44 | 0.00 | 0.2 | 45.0 | 54.9 |
| 17 | LTM1-15 Pl1 1 | 61.78 | 0.01 | 23.42 | 0.09 | 5.19 | 8.71 | 0.01 | 99.22 | 2.76 | 1.23 | 0.25 | 0.75 | 0.00 | 0.1 | 75.2 | 24.8 |
| 18 | LTM1-15 Pl1 2 | 62.21 | 0.01 | 23.47 | 0.03 | 5.29 | 8.89 | n.d. | 99.90 | 2.76 | 1.23 | 0.25 | 0.76 | 0.00 | 0.0 | 75.2 | 24.8 |
| 19 | LTM1-15 Pl2 1 | 63.92 | 0.03 | 22.14 | 0.11 | 3.80 | 9.30 | 0.03 | 99.33 | 2.84 | 1.16 | 0.18 | 0.80 | 0.00 | 0.1 | 81.5 | 18.4 |
| 20 | LTM1-15 Pl2 2 | 63.65 | 0.01 | 22.34 | 0.12 | 3.96 | 9.14 | 0.03 | 99.25 | 2.83 | 1.17 | 0.19 | 0.79 | 0.00 | 0.2 | 80.5 | 19.3 |
| 21 | LTM1-15 Pl3 1 | 60.51 | 0.03 | 24.20 | 0.05 | 6.09 | 8.25 | 0.01 | 99.14 | 2.71 | 1.28 | 0.29 | 0.72 | 0.00 | 0.1 | 71.0 | 28.9 |
| 22 | LTM1-15 Pl3 2 | 61.06 | n.d. | 24.03 | 0.07 | 5.84 | 8.48 | 0.02 | 99.50 | 2.73 | 1.26 | 0.28 | 0.73 | 0.00 | 0.1 | 72.3 | 27.5 |

Note. Results of electron-microprobe analyses conducted by wavelength-dispersive spectrometry are listed in weight %. Apfu: atoms per formula unit based on eight oxygen atoms. n.d.: not detected (below detection limits). Or: orthoclase; Ab: albite; An: anorthite.

**Table 4.** Compositions of grains of chromian spinels in the orthopyroxenite zone of the Lotmvara-I sill, Kola Peninsula.

| # | Sample | $TiO_2$ | $Al_2O_3$ | $Cr_2O_3$ | $V_2O_3$ | $Fe_2O_3$ (calc) | FeO (calc) | FeO (tot) | MnO | MgO | ZnO | NiO | Total |
|---|---|---|---|---|---|---|---|---|---|---|---|---|---|
| 1 | LTM1-11 Chr1 1 | 1.29 | 16.88 | 45.48 | 0.17 | 3.08 | 26.64 | 29.41 | 0.35 | 5.38 | 0.64 | 0.04 | 99.94 |
| 2 | LTM1-11 Chr1 2 | 0.18 | 17.71 | 45.14 | 0.14 | 4.70 | 25.30 | 29.53 | 0.34 | 5.62 | 0.72 | 0.02 | 99.87 |
| 3 | LTM1-11 Chr2 1 | 0.05 | 13.30 | 49.37 | 0.21 | 5.66 | 25.34 | 30.44 | 0.37 | 5.15 | 0.56 | 0.06 | 100.09 |
| 4 | LTM1-11 Chr2 2 | 0.05 | 13.31 | 48.85 | 0.15 | 6.03 | 25.09 | 30.51 | 0.36 | 5.19 | 0.66 | 0.06 | 99.74 |
| 5 | LTM1-11 Chr3 1 | 1.74 | 14.33 | 48.25 | 0.13 | 2.31 | 27.99 | 30.07 | 0.36 | 4.55 | 0.74 | 0.03 | 100.44 |
| 6 | LTM1-11 Chr3 2 | 0.77 | 14.47 | 49.12 | 0.11 | 3.45 | 27.24 | 30.34 | 0.35 | 4.56 | 0.74 | 0.02 | 100.82 |
| 7 | LTM1-14 Chr1 1 | 0.09 | 12.33 | 51.25 | 0.13 | 5.29 | 25.30 | 30.06 | 0.33 | 5.17 | 0.73 | 0.03 | 100.63 |
| 8 | LTM1-14 Chr1 2 | 0.12 | 12.41 | 51.21 | 0.18 | 4.96 | 25.34 | 29.80 | 0.33 | 5.11 | 0.75 | 0.04 | 100.44 |
| 9 | LTM1-14 Chr2 1 | 0.08 | 12.09 | 51.24 | 0.16 | 5.57 | 25.60 | 30.61 | 0.36 | 4.92 | 0.77 | 0.04 | 100.82 |
| 10 | LTM1-14 Chr2 2 | 0.09 | 12.13 | 51.19 | 0.16 | 5.41 | 25.68 | 30.55 | 0.35 | 4.83 | 0.85 | 0.04 | 100.73 |
| 11 | LTM1-14 Chr3 1 | 0.13 | 12.42 | 51.27 | 0.34 | 4.46 | 26.60 | 30.61 | 0.35 | 4.35 | 0.77 | n.d. | 100.69 |
| 12 | LTM1-14 Chr3 2 | 0.10 | 12.34 | 51.39 | 0.28 | 4.42 | 26.62 | 30.60 | 0.38 | 4.26 | 0.78 | n.d. | 100.59 |
| 13 | LTM1-15 Chr1 1 | 0.16 | 17.64 | 48.71 | 0.20 | 1.34 | 24.81 | 26.02 | 0.31 | 5.78 | 1.11 | 0.02 | 100.09 |
| 14 | LTM1-15 Chr1 2 | 0.11 | 17.47 | 48.61 | 0.23 | 1.58 | 24.94 | 26.36 | 0.32 | 5.67 | 1.04 | 0.01 | 99.97 |
| 15 | LTM1-15 Chr2 1 | 0.25 | 14.16 | 51.26 | 0.16 | 2.96 | 25.53 | 28.20 | 0.36 | 5.46 | 0.42 | 0.06 | 100.62 |
| 16 | LTM1-15 Chr2 2 | 0.26 | 13.97 | 50.68 | 0.15 | 2.78 | 25.47 | 27.96 | 0.35 | 5.28 | 0.36 | 0.05 | 99.34 |

**Table 4.** *Cont.*

| # | Sample | $TiO_2$ | $Al_2O_3$ | $Cr_2O_3$ | $V_2O_3$ | $Fe_2O_3$ (calc) | FeO (calc) | FeO (tot) | MnO | MgO | ZnO | NiO | Total |
|---|---|---|---|---|---|---|---|---|---|---|---|---|---|
| 17 | LTM1-15 Chr3 1 | 0.83 | 17.21 | 47.75 | 0.23 | 0.92 | 25.10 | 25.93 | 0.27 | 5.88 | 0.95 | 0.03 | 99.16 |
| 18 | LTM1-15 Chr3 2 | 0.67 | 17.45 | 48.21 | 0.26 | 1.26 | 24.95 | 26.08 | 0.31 | 6.05 | 1.00 | 0.05 | 100.19 |
| *apfu* | | | | | | | | | | | | | |
| # | Ti | Al | Cr | V | $Fe^{3+}$ | $Fe^{2+}$ | Mn | Mg | Zn | Ni | Cr# | Mg# | $Fe^{3+}$# |
| 1 | 0.032 | 0.66 | 1.19 | 0.004 | 0.08 | 0.74 | 0.01 | 0.27 | 0.02 | 0.001 | 64.4 | 26.2 | 9.4 |
| 2 | 0.004 | 0.69 | 1.18 | 0.004 | 0.12 | 0.70 | 0.01 | 0.28 | 0.02 | 0.001 | 63.1 | 28.1 | 14.3 |
| 3 | 0.001 | 0.53 | 1.32 | 0.006 | 0.14 | 0.72 | 0.01 | 0.26 | 0.01 | 0.002 | 71.3 | 26.3 | 16.7 |
| 4 | 0.001 | 0.53 | 1.31 | 0.004 | 0.15 | 0.71 | 0.01 | 0.26 | 0.02 | 0.002 | 71.1 | 26.7 | 17.8 |
| 5 | 0.044 | 0.57 | 1.28 | 0.003 | 0.06 | 0.79 | 0.01 | 0.23 | 0.02 | 0.001 | 69.3 | 22.2 | 6.9 |
| 6 | 0.019 | 0.57 | 1.30 | 0.003 | 0.09 | 0.76 | 0.01 | 0.23 | 0.02 | 0.001 | 69.5 | 22.8 | 10.2 |
| 7 | 0.002 | 0.49 | 1.37 | 0.004 | 0.13 | 0.71 | 0.01 | 0.26 | 0.02 | 0.001 | 73.6 | 26.4 | 15.8 |
| 8 | 0.003 | 0.49 | 1.37 | 0.005 | 0.13 | 0.72 | 0.01 | 0.26 | 0.02 | 0.001 | 73.5 | 26.2 | 15.0 |
| 9 | 0.002 | 0.48 | 1.37 | 0.004 | 0.14 | 0.72 | 0.01 | 0.25 | 0.02 | 0.001 | 74.0 | 25.2 | 16.4 |
| 10 | 0.002 | 0.48 | 1.37 | 0.004 | 0.14 | 0.73 | 0.01 | 0.24 | 0.02 | 0.001 | 73.9 | 24.9 | 15.9 |
| 11 | 0.003 | 0.50 | 1.37 | 0.009 | 0.11 | 0.75 | 0.01 | 0.22 | 0.02 | 0.000 | 73.5 | 22.3 | 13.1 |
| 12 | 0.003 | 0.49 | 1.38 | 0.008 | 0.11 | 0.76 | 0.01 | 0.22 | 0.02 | 0.000 | 73.6 | 22.0 | 13.0 |
| 13 | 0.004 | 0.69 | 1.27 | 0.005 | 0.03 | 0.68 | 0.01 | 0.28 | 0.03 | 0.001 | 64.9 | 29.1 | 4.6 |
| 14 | 0.003 | 0.68 | 1.27 | 0.006 | 0.04 | 0.69 | 0.01 | 0.28 | 0.03 | 0.000 | 65.1 | 28.6 | 5.4 |
| 15 | 0.006 | 0.56 | 1.35 | 0.004 | 0.07 | 0.71 | 0.01 | 0.27 | 0.01 | 0.002 | 70.8 | 27.3 | 9.4 |
| 16 | 0.007 | 0.56 | 1.36 | 0.004 | 0.07 | 0.72 | 0.01 | 0.27 | 0.01 | 0.001 | 70.9 | 26.7 | 8.9 |
| 17 | 0.021 | 0.67 | 1.26 | 0.006 | 0.02 | 0.70 | 0.01 | 0.29 | 0.02 | 0.001 | 65.1 | 29.2 | 3.2 |
| 18 | 0.016 | 0.68 | 1.25 | 0.007 | 0.03 | 0.69 | 0.01 | 0.30 | 0.02 | 0.001 | 65.0 | 29.9 | 4.3 |

Note. Results of electron-microprobe analyses conducted by wavelength-dispersive spectrometry are listed in weight %. Apfu: atoms per formula unit based on four oxygen atoms. n.d.: not detected (below detection limits). Chr: chromian spinel. The index Chr# is defined as 100Cr/(Cr + Al), the index $Fe^{3+}$# as $100Fe^{3+}/(Fe^{3+} + Fe^{2+})$, and the index Mg# as $100Mg/(Mg + Fe^{2+} + Mn)$.

The corona texture occurs in specimens of plagioclase-bearing orthopyroxenite that are unmetamorphosed (Figures 6–8). The corona involves a partial rim of clinopyroxene of the augite–diopside series [19], with the following range of compositions: $Wo_{35.7–46.9}En_{44.8–51.9}Fs_{6.3–11.2}Aeg_{1.1–2.1}$; Mg# 78.4–83.0 (#26–31, Table 1). The partial rim of clinopyroxene is mantled by a partial rim of deuterically induced tremolite (#6–22, Table 2), plagioclase (#10–16, Table 3), and small inclusions of quartz. Grains of disseminated chromite contain substantial levels of Mg in this rock: 4.26–5.17 wt.% MgO (#7–12, Table 4).

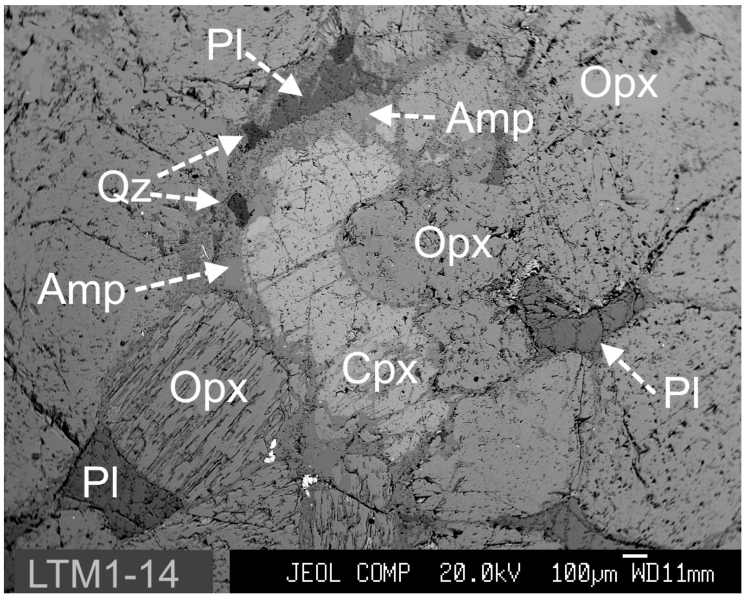


**Figure 8.** A BSE image shows a corona-type texture in the orthopyroxenite zone of the Lotmvara-I sill. It is represented by the development of a partial rim of clinopyroxene (Cpx) around a core grain of orthopyroxene (Opx). The Cpx shell itself is surrounded partially by a composite rim of amphibole (Amp), plagioclase (Pl), and quartz (Qz). The location of this sample, Ltm1-14 (Figure 6b), is shown in Figure 1.

### *3.2. Corona-Type Texture in the Chapesvara-I Sill*

Figure 9a shows an interesting example of a composite corona with the following sequence of crystallization, inferred from early to late phases in the paragenesis: Ol → Opx → Cpx → Pl → Amp. This texture occurs locally in a fresh specimen of fine-grained harzburgite (CHP-10) from the sill (Figure 6d). This rock sample was clearly not affected by any metamorphic influences or transformations (Figure 9b) and thus preserves its original state and texture. The corona-forming association is represented by olivine in the core; it has an elevated magnesium content (Mg# 86.0–86.7). There follow narrow or broader partial rims of orthopyroxene (Mg# 86.0–88.0), clinopyroxene ($Wo_{38.7–43.4}En_{47.4–51.9}Fs_{6.2–6.9}Aeg_{2.5–3.1}$), plagioclase ($An_{39.7–52.1}Ab_{47.8–60.2}Or_{0.1–0.2}$) and an uncommon variant of aluminous sodic–calcic amphibole: $Ca_{1.20–1.21}Na_{1.08–1.09}(Mg_{3.53–3.78}Fe^{2+}{}_{0.47–0.58})_{\Sigma 5.00}{}^{VI}Al_{0.75–1.00}(Si_{5.59–6.00}Al_{2.00–2.41})(OH)_{1.86–1.88}$ (#24–27 in Table 5), cf. nomenclature in [20]. The magnesium content of the augite is comparatively high (Mg# 89.9–91.7) owing to the presence of minor amounts of calculated $Fe^{3+}$. Members of the spinel group are relatively magnesian in this rock: MgO 6.59–7.36 wt.% (#28–33 in Table 5).

**Table 5.** Compositions of minerals in a fine-grained harzburgite with a corona-type texture in the Chapesvara-I ultrabasic sill, Kola Peninsula.

| # | Sample | | $SiO_2$ | $TiO_2$ | $Al_2O_3$ | $Cr_2O_3$ | $V_2O_3$ | FeO | MnO | MgO | CaO | ZnO | NiO | $Na_2O$ | $K_2O$ | Total |
|---|---|---|---|---|---|---|---|---|---|---|---|---|---|---|---|---|
| 1 | CHP10 Ol1 1 | Ol | 40.04 | n.d. | n.d. | 0.01 | n.d. | 13.00 | 0.20 | 46.71 | 0.01 | n.d. | 0.33 | n.d. | n.d. | 100.30 |
| 2 | CHP10 Ol1 2 | | 39.96 | n.d. | n.d. | 0.02 | n.d. | 12.77 | 0.18 | 46.28 | 0.02 | n.d. | 0.31 | n.d. | n.d. | 99.54 |
| 3 | CHP10 Ol2 1 | | 40.13 | n.d. | n.d. | 0.12 | n.d. | 12.63 | 0.18 | 46.59 | 0.01 | n.d. | 0.33 | n.d. | n.d. | 99.98 |
| 4 | CHP10 Ol2 2 | | 40.17 | n.d. | n.d. | 0.02 | n.d. | 12.94 | 0.20 | 46.63 | 0.04 | n.d. | 0.32 | n.d. | n.d. | 100.33 |
| 5 | CHP10 Ol3 1 | | 39.71 | n.d. | n.d. | 0.02 | n.d. | 12.66 | 0.17 | 46.52 | 0.01 | n.d. | 0.34 | n.d. | n.d. | 99.43 |
| 6 | CHP10 Ol3 2 | | 40.03 | n.d. | n.d. | 0.01 | n.d. | 12.56 | 0.16 | 46.59 | 0.01 | n.d. | 0.35 | n.d. | n.d. | 99.70 |
| 7 | CHP10 Ol4 | | 40.28 | n.d. | n.d. | 0.02 | n.d. | 13.21 | 0.17 | 46.17 | 0.04 | n.d. | 0.32 | n.d. | n.d. | 100.21 |
| 8 | CHP10 Opx1 1 | Opx | 56.50 | 0.04 | 1.36 | 0.73 | n.d. | 7.53 | 0.17 | 31.83 | 1.59 | n.d. | n.d. | 0.13 | 0.01 | 99.89 |
| 9 | CHP10 Opx1 2 | | 56.63 | 0.07 | 1.37 | 0.72 | n.d. | 7.67 | 0.17 | 31.97 | 1.33 | n.d. | n.d. | 0.07 | n.d. | 99.99 |
| 10 | CHP10 Opx2 1 | | 56.70 | 0.05 | 1.19 | 0.70 | n.d. | 7.17 | 0.16 | 32.13 | 1.37 | n.d. | n.d. | 0.07 | n.d. | 99.54 |
| 11 | CHP10 Opx2 2 | | 56.17 | 0.05 | 1.43 | 0.66 | n.d. | 7.85 | 0.18 | 31.53 | 1.41 | n.d. | n.d. | 0.06 | 0.01 | 99.34 |
| 12 | CHP10 Opx3 1 | | 56.61 | 0.06 | 1.24 | 0.72 | n.d. | 7.00 | 0.15 | 32.54 | 1.24 | n.d. | n.d. | 0.05 | n.d. | 99.60 |
| 13 | CHP10 Opx3 2 | | 55.50 | 0.07 | 2.22 | 0.75 | n.d. | 7.92 | 0.19 | 30.42 | 2.37 | n.d. | n.d. | 0.07 | n.d. | 99.49 |
| 14 | CHP10 Cpx1 1 | Cpx | 52.98 | 0.19 | 2.81 | 1.32 | n.d. | 3.79 | 0.13 | 16.70 | 21.16 | n.d. | n.d. | 0.84 | 0.01 | 99.91 |
| 15 | CHP10 Cpx1 2 | | 52.80 | 0.30 | 2.82 | 1.15 | n.d. | 3.98 | 0.14 | 16.97 | 20.82 | n.d. | n.d. | 0.76 | n.d. | 99.73 |
| 16 | CHP10 Cpx2 1 | | 52.60 | 0.18 | 3.33 | 1.27 | n.d. | 3.87 | 0.15 | 16.51 | 20.92 | n.d. | n.d. | 0.76 | n.d. | 99.59 |
| 17 | CHP10 Cpx2 2 | | 52.44 | 0.21 | 3.30 | 1.26 | n.d. | 3.93 | 0.10 | 16.58 | 20.97 | n.d. | n.d. | 0.72 | n.d. | 99.51 |
| 18 | CHP10 Cpx3 1 | | 52.85 | 0.17 | 2.89 | 1.27 | n.d. | 4.22 | 0.13 | 18.37 | 19.04 | n.d. | n.d. | 0.69 | 0.01 | 99.63 |
| 19 | CHP10 Cpx3 2 | | 52.36 | 0.17 | 2.94 | 1.34 | n.d. | 3.81 | 0.14 | 16.63 | 21.10 | n.d. | n.d. | 0.70 | n.d. | 99.20 |
| 20 | CHP10 Pl1 1 | Pl | 55.94 | 0.08 | 27.30 | n.d. | n.d. | 0.08 | 0.02 | 0.06 | 9.72 | n.d. | n.d. | 6.45 | 0.04 | 99.69 |
| 21 | CHP10 Pl1 2 | | 57.37 | 0.07 | 26.41 | n.d. | n.d. | 0.14 | 0.01 | 0.01 | 8.75 | n.d. | n.d. | 7.32 | 0.02 | 100.10 |
| 22 | CHP10 Pl2 1 | | 54.15 | 0.07 | 28.55 | n.d. | n.d. | 0.12 | 0.01 | 0.00 | 11.09 | n.d. | n.d. | 5.63 | 0.02 | 99.63 |
| 23 | CHP10 Pl2 2 | | 54.38 | 0.05 | 28.23 | 0.03 | n.d. | 0.11 | n.d. | 0.09 | 10.98 | n.d. | n.d. | 5.79 | 0.04 | 99.70 |
| 24 | CHP10 Amp1 1 | Amp | 40.63 | 0.03 | 20.68 | n.d. | n.d. | 5.02 | 0.15 | 17.91 | 8.12 | n.d. | n.d. | 4.24 | 0.19 | 96.98 |
| 25 | CHP10 Amp1 2 | | 41.55 | 0.06 | 20.43 | n.d. | n.d. | 4.89 | 0.11 | 17.52 | 8.00 | n.d. | n.d. | 4.46 | 0.25 | 97.26 |
| 26 | CHP10 Amp2 1 | | 43.49 | 0.04 | 17.07 | 0.01 | n.d. | 4.74 | 0.13 | 18.84 | 8.28 | n.d. | n.d. | 4.36 | 0.19 | 97.13 |
| 27 | CHP10 Amp2 2 | | 42.46 | 0.08 | 17.71 | 0.03 | n.d. | 4.55 | 0.08 | 18.52 | 8.57 | n.d. | n.d. | 4.40 | 0.48 | 96.88 |
| 28 | CHP10 Chr1 1 | Chr | n.d. | 0.57 | 19.09 | 39.13 | 0.27 | 33.64 | 0.41 | 6.77 | n.d. | 0.21 | 0.19 | n.d. | n.d. | 100.27 |
| 29 | CHP10 Chr1 2 | | n.d. | 0.64 | 18.87 | 39.30 | 0.27 | 33.47 | 0.40 | 6.63 | n.d. | 0.16 | 0.16 | n.d. | n.d. | 99.91 |
| 30 | CHP10 Chr2 1 | | n.d. | 4.20 | 17.17 | 37.87 | 0.27 | 33.22 | 0.43 | 6.59 | n.d. | 0.14 | 0.11 | n.d. | n.d. | 100.00 |
| 31 | CHP10 Chr2 2 | | n.d. | 2.54 | 17.19 | 39.09 | 0.26 | 32.98 | 0.41 | 6.68 | n.d. | 0.13 | 0.17 | n.d. | n.d. | 99.45 |
| 32 | CHP10 Chr3 1 | | n.d. | 0.91 | 19.73 | 39.40 | 0.20 | 31.26 | 0.40 | 7.36 | n.d. | 0.21 | 0.15 | n.d. | n.d. | 99.62 |
| 33 | CHP10 Chr3 2 | | n.d. | 0.50 | 19.67 | 39.18 | 0.26 | 32.31 | 0.40 | 7.27 | n.d. | 0.19 | 0.18 | n.d. | n.d. | 99.95 |

Note. Results of electron-microprobe analyses conducted by wavelength-dispersive spectrometry are listed in weight %. n.d.: not detected (below detection limits). Ol: olivine; Opx: orthopyroxene; Cpx: clinopyroxene; Pl: plagioclase; Amp: amphibole; Chr: chromian spinel.

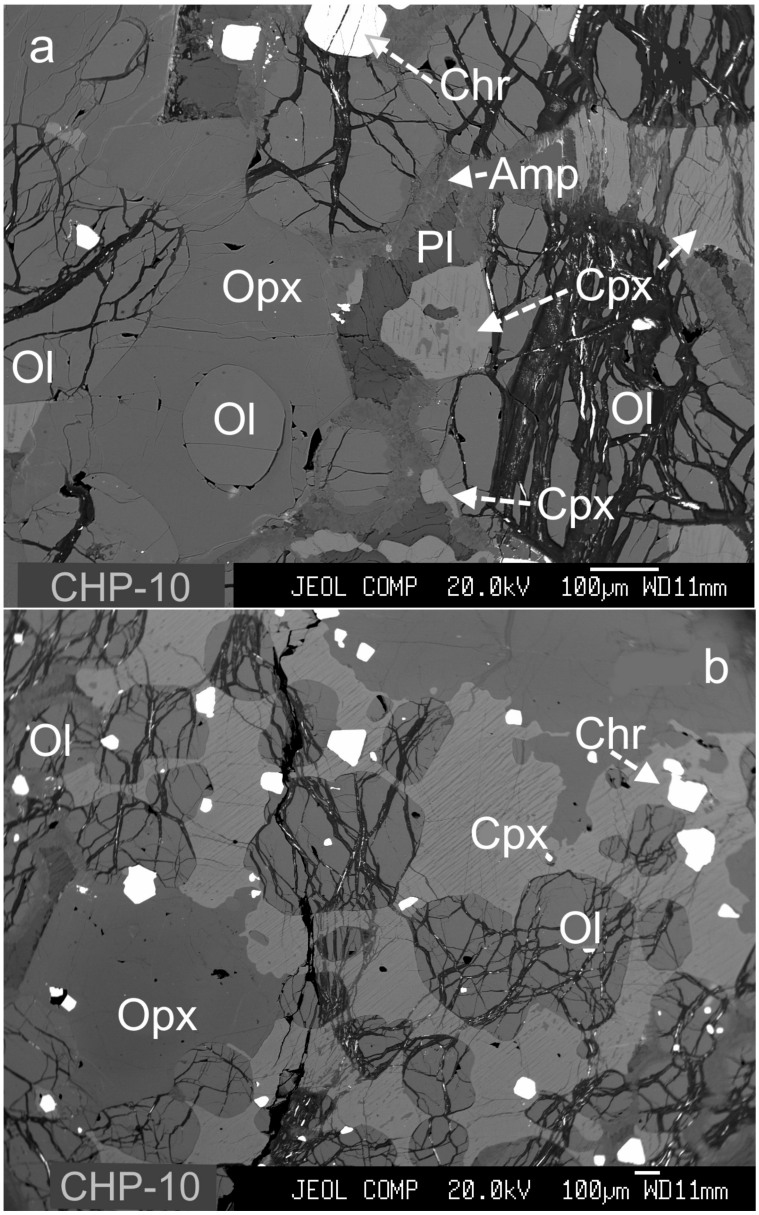


**Figure 9.** (**a**,**b**). A BSE image shows a corona-type texture composed of olivine (Ol), orthopyroxene (Opx), clinopyroxene (Cpx), and amphibole (Amp), in a specimen of fresh harzburgite, another fragment of which is displayed in Figure 6b, from the Chapesvara-I sill (see Figure 6b for sample location).

### *3.3. Corona-Type Texture in the Lyavaraka Complex*

Occurrences of a symplectitic corona (Figure 10a,b) are documented in a specimen of plagioclase-bearing orthopyroxenite in sample LVR-21a (Figure 6e), collected in the Zone of Recurrent Ol + Cpx + Pl (III), cf. [6]. Again, this rock is fresh and undeformed; it does not exhibit evidence of regional metamorphic or tectonic influence. It consists of well-formed grains of orthopyroxene ($Wo_{2.8}En_{78.9}Fs_{18.1}$; Mg# 80.0), which strongly dominates, with subordinate quantities of plagioclase, $An_{44.2–48.5}Ab_{50.8–55.3}Or_{0.5–0.7}$ (up to 10–15% of the mode), and minor clinopyroxene ($Wo_{45.5–47.7}En_{43.6–45.2}Fs_{5.9–6.8}Aeg_{0.2}$; Mg# 86.5–88.0). The values of the Mg# index are somewhat higher in the compositions of the clinopyroxene grains, which may represent primocrysts in this rock. The amphibole rim, containing micrometer-sized inclusions of symplectitic quartz, corresponds to an aluminous variant of magnesiohornblende: 6.99–10.74 wt.% $Al_2O_3$ (#11–15 in Table 6).

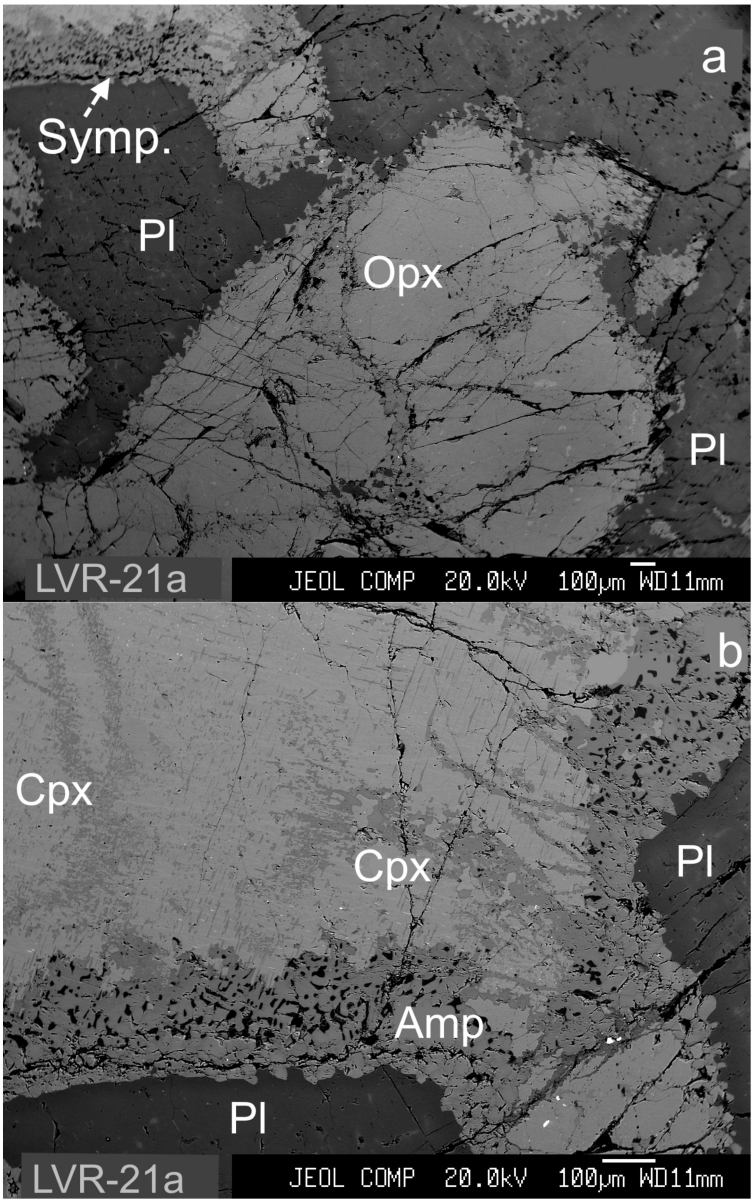


**Figure 10.** (**a**,**b**). BSE images of corona-type texture in a plagioclase-bearing orthopyroxenite of the Lyavaraka complex (Figure 6e). The symbols are: Opx for orthopyroxene, Cpx for clinopyroxene, Amp for amphibole, and Chr for chromian spinel. The myrmekite-type shell consists of amphibole with micrometer-sized inclusions of quartz (black). The sample location (LVR-21a) is shown in Figure 5.

**Table 6.** Compositions of minerals in a Pl-bearing orthopyroxenite with a corona-type texture in the Lyavaraka ultrabasic complex, Kola Peninsula.

| # | Sample | | $SiO_2$ | $TiO_2$ | $Al_2O_3$ | $Cr_2O_3$ | FeO | MnO | MgO | CaO | $Na_2O$ | $K_2O$ | Total |
|---|---|---|---|---|---|---|---|---|---|---|---|---|---|
| 1 | LVR21A-1 | Opx | 55.12 | 0.04 | 1.85 | 0.49 | 11.46 | 0.22 | 28.63 | 1.44 | 0.06 | 0.01 | 99.30 |
| 2 | LVR21A-1 | Cpx | 53.50 | 0.20 | 2.53 | 0.49 | 3.77 | 0.12 | 15.18 | 22.93 | 0.75 | n.d. | 99.47 |
| 3 | LVR21A-2 | | 53.50 | 0.20 | 2.60 | 0.48 | 3.75 | 0.13 | 15.24 | 22.83 | 0.81 | n.d. | 99.54 |
| 4 | LVR21A-3 | | 53.56 | 0.17 | 2.32 | 0.51 | 3.75 | 0.13 | 15.24 | 22.91 | 0.77 | 0.01 | 99.38 |
| 5 | LVR21A-4 | | 53.63 | 0.15 | 2.23 | 0.47 | 3.58 | 0.13 | 15.36 | 23.29 | 0.71 | 0.01 | 99.57 |
| 6 | LVR21A-5 | | 53.69 | 0.18 | 2.25 | 0.43 | 4.11 | 0.15 | 15.96 | 22.35 | 0.66 | n.d. | 99.78 |
| 7 | LVR21A-1 | Pl | 55.77 | n.d. | 27.41 | n.d. | 0.02 | n.d. | n.d. | 9.52 | 6.52 | 0.09 | 99.34 |
| 8 | LVR21A-2 | | 55.76 | n.d. | 27.46 | n.d. | 0.04 | n.d. | n.d. | 9.58 | 6.63 | 0.09 | 99.56 |
| 9 | LVR21A-3 | | 54.88 | n.d. | 28.02 | n.d. | 0.02 | n.d. | n.d. | 10.26 | 5.93 | 0.13 | 99.22 |
| 10 | LVR21A-4 | | 56.16 | n.d. | 27.72 | n.d. | 0.03 | n.d. | n.d. | 9.79 | 5.90 | 0.13 | 99.71 |
| 11 | LVR21A Amp1 1 | Amp | 48.02 | 0.91 | 10.60 | 0.37 | 6.47 | 0.07 | 16.41 | 12.15 | 1.32 | 0.71 | 97.02 |
| 12 | LVR21A Amp1 2 | | 49.43 | 0.78 | 9.02 | 0.28 | 6.03 | 0.09 | 17.36 | 12.19 | 1.10 | 0.58 | 96.86 |

**Table 6.** *Cont.*

| # | Sample | $SiO_2$ | $TiO_2$ | $Al_2O_3$ | $Cr_2O_3$ | FeO | MnO | MgO | CaO | $Na_2O$ | $K_2O$ | Total |
|---|---|---|---|---|---|---|---|---|---|---|---|---|
| 13 | LVR21A Amp2 1 | 47.94 | 0.91 | 10.51 | 0.39 | 6.41 | 0.08 | 16.48 | 12.16 | 1.39 | 0.75 | 97.01 |
| 14 | LVR21A Amp2 2 | 48.15 | 0.91 | 10.74 | 0.40 | 6.47 | 0.10 | 16.40 | 12.09 | 1.33 | 0.75 | 97.33 |
| 15 | LVR21A Amp2a | 51.82 | 0.56 | 6.99 | 0.43 | 5.28 | 0.09 | 18.41 | 12.27 | 0.88 | 0.36 | 97.09 |

Note. Results of electron-microprobe analyses done by wavelength-dispersive spectrometry are listed in weight %. n.d.: not detected (below detection limits). Opx: orthopyroxene; Cpx: clinopyroxene; Pl: plagioclase; Amp: amphibole.

### *3.4. Lamellae of Phlogopite and $Al_2SiO_5$ Hosted by Plagioclase at Lotmvara-I*

We note unusual occurrences of lamellar grains of phlogopite (#1–4 and 5–7 in Table 7) and, more surprisingly, a phase of $Al_2SiO_5$ composition (#8–26 and 27, 28 in Table 7) (Figure 11a,b). They occur in mutual association as more or less randomly oriented inclusions (Figure 11b) hosted by interstitial grains of plagioclase in specimens of orthopyroxenite (Figure 6c). Some of these inclusions are aligned (cf. the upper part of the BSE image shown in Figure 11a), possibly a reflection of their attachment on a growth surface of the plagioclase host. Interestingly, small grains of chlorapatite (#1–3 in Table 8; sample LTM1-15) also are present in this association.

**Table 7.** Compositions of micrometer-sized inclusions of phlogopite and $Al_2SiO_5$ hosted by grains of plagioclase in the orthopyroxenite zone of the Lotmvara-I sill, Kola Peninsula.

| # | Sample | Mineral | $SiO_2$ | $TiO_2$ | $Al_2O_3$ | $Cr_2O_3$ | FeO | MnO | MgO | CaO | $Na_2O$ | $K_2O$ | Total |
|---|---|---|---|---|---|---|---|---|---|---|---|---|---|
| 1 | LTM1-11 Inc1 | Phl | 39.89 | 0.34 | 19.26 | 0.03 | 3.54 | 0.01 | 20.30 | 0.38 | 0.73 | 8.81 | 93.29 |
| 2 | LTM1-11 inc2 | - | 45.27 | 0.41 | 21.73 | n.d. | 2.98 | 0.02 | 15.72 | 1.95 | 2.25 | 7.12 | 97.44 |
| 3 | LTM1-11 inc4 | - | 41.03 | 0.40 | 23.04 | 0.01 | 3.25 | 0.02 | 18.57 | 0.47 | 0.94 | 7.88 | 95.60 |
| 4 | LTM1-11 inc5 | - | 40.86 | 0.45 | 20.63 | 0.02 | 3.60 | 0.03 | 19.57 | 0.52 | 0.76 | 8.51 | 94.93 |
| 5 | LTM1-15 inc3 | - | 44.03 | 0.59 | 19.01 | 0.26 | 2.91 | 0.02 | 18.19 | 0.86 | 2.76 | 6.39 | 95.01 |
| 6 | LTM1-15 inc4 | - | 42.29 | 0.70 | 18.35 | 0.03 | 3.37 | 0.01 | 20.61 | 0.51 | 2.34 | 7.25 | 95.46 |
| 7 | LTM1-15 inc5 | - | 40.37 | 0.69 | 17.60 | 0.34 | 3.24 | 0.02 | 20.14 | 0.29 | 1.69 | 7.38 | 91.77 |
| 8 | LTM1-11 Inc1 1 | $Al_2SiO_5$ | 39.55 | n.d. | 61.17 | n.d. | 0.30 | n.d. | n.d. | 0.25 | 0.41 | 0.01 | 101.69 |
| 9 | LTM1-11 Inc1 2 | - | 39.30 | n.d. | 61.11 | n.d. | 0.30 | n.d. | n.d. | 0.23 | 0.37 | 0.02 | 101.33 |
| 10 | LTM1-11 Inc2 1 | - | 39.77 | 0.01 | 55.36 | n.d. | 0.24 | n.d. | n.d. | 1.56 | 0.54 | 0.01 | 97.48 |
| 11 | LTM1-11 Inc2 2 | - | 39.24 | 0.03 | 55.82 | n.d. | 0.24 | n.d. | n.d. | 1.45 | 0.50 | 0.01 | 97.28 |
| 12 | LTM1-11 Inc4 | - | 39.84 | n.d. | 57.70 | n.d. | 0.27 | n.d. | n.d. | 1.18 | 0.49 | 0.01 | 99.48 |
| 13 | LTM1-11 Inc5 | - | 38.92 | n.d. | 61.32 | n.d. | 0.38 | n.d. | n.d. | 0.15 | 0.12 | 0.17 | 101.05 |
| 14 | LTM1-11 Inc7 | - | 38.43 | n.d. | 62.59 | n.d. | 0.34 | n.d. | n.d. | 0.10 | 0.05 | n.d. | 101.50 |
| 15 | LTM1-11 Inc8 | - | 39.27 | n.d. | 58.91 | n.d. | 0.33 | n.d. | n.d. | 0.84 | 0.33 | 0.01 | 99.69 |
| 16 | LTM1-11 Inc9 1 | - | 36.88 | 0.01 | 62.94 | n.d. | 0.37 | n.d. | n.d. | 0.09 | n.d. | 0.01 | 100.30 |
| 17 | LTM1-11 Inc9 2 | - | 36.83 | 0.03 | 62.89 | n.d. | 0.38 | n.d. | n.d. | 0.10 | 0.01 | n.d. | 100.24 |
| 18 | LTM1-11 Inc10 1 | - | 40.84 | 0.01 | 53.62 | n.d. | 0.24 | n.d. | n.d. | 2.20 | 0.95 | 0.01 | 97.86 |
| 19 | LTM1-11 Inc10 2 | - | 40.63 | 0.02 | 53.88 | n.d. | 0.22 | n.d. | n.d. | 2.02 | 0.91 | 0.01 | 97.68 |
| 20 | LTM1-11 Inc11 3 | - | 38.42 | 0.02 | 58.77 | n.d. | 0.32 | n.d. | n.d. | 0.82 | 0.61 | 0.02 | 98.98 |
| 21 | LTM1-11 Inc12 | - | 40.18 | 0.02 | 55.15 | n.d. | 0.27 | n.d. | n.d. | 1.81 | 0.93 | n.d. | 98.34 |
| 22 | LTM1-11 Inc13 | - | 37.08 | n.d. | 61.19 | n.d. | 0.35 | n.d. | n.d. | 0.18 | 0.24 | 0.10 | 99.14 |
| 23 | LTM1-11 Inc14 1 | - | 36.98 | n.d. | 63.08 | n.d. | 0.30 | n.d. | n.d. | 0.04 | 0.03 | 0.01 | 100.42 |
| 24 | LTM1-11 Inc14 2 | - | 36.76 | 0.02 | 62.61 | n.d. | 0.30 | n.d. | n.d. | 0.05 | n.d. | 0.01 | 99.74 |
| 25 | LTM1-11 Inc15 | - | 37.30 | n.d. | 62.45 | n.d. | 0.30 | n.d. | n.d. | 0.16 | 0.19 | 0.02 | 100.43 |
| 26 | LTM1-11 Inc16 | - | 39.83 | n.d. | 55.49 | n.d. | 0.25 | n.d. | n.d. | 1.65 | 0.79 | n.d. | 98.01 |
| 27 | LTM1-15 inc1 | - | 36.49 | 0.03 | 62.13 | n.d. | 0.16 | n.d. | n.d. | 0.05 | 0.03 | n.d. | 98.90 |
| 28 | LTM1-15 inc3 | - | 37.29 | 0.01 | 61.38 | n.d. | 0.10 | n.d. | n.d. | 0.09 | 0.16 | 0.02 | 99.05 |

***apfu***

| # | Si | Ti | $^{[4]}Al$ | Al | Al+Si | $Fe^{2+}$ | Mn | Mg | Ca | Na | K |
|---|---|---|---|---|---|---|---|---|---|---|---|
| 1 | 5.69 | 0.04 | 2.31 | 0.92 | - | 0.42 | <0.01 | 4.31 | 0.06 | 0.20 | 1.60 |
| 2 | 6.06 | 0.04 | 1.94 | 1.49 | - | 0.33 | <0.01 | 3.14 | 0.28 | 0.58 | 1.22 |
| 3 | 5.63 | 0.04 | 2.37 | 1.36 | - | 0.37 | <0.01 | 3.80 | 0.07 | 0.25 | 1.38 |
| 4 | 5.70 | 0.05 | 2.30 | 1.09 | - | 0.42 | <0.01 | 4.07 | 0.08 | 0.21 | 1.51 |
| 5 | 6.06 | 0.06 | 1.94 | 1.15 | - | 0.34 | <0.01 | 3.73 | 0.13 | 0.74 | 1.12 |
| 6 | 5.85 | 0.07 | 2.15 | 0.84 | - | 0.39 | <0.01 | 4.25 | 0.08 | 0.63 | 1.28 |
| 7 | 5.83 | 0.07 | 2.17 | 0.83 | - | 0.39 | <0.01 | 4.34 | 0.04 | 0.47 | 1.36 |
| 8 | 1.05 | 0.00 | - | 1.92 | 2.97 | 0.01 | 0.00 | 0.00 | 0.01 | 0.02 | 0.00 |
| 9 | 1.05 | 0.00 | - | 1.92 | 2.97 | 0.01 | 0.00 | 0.00 | 0.01 | 0.02 | 0.00 |
| 10 | 1.11 | 0.00 | - | 1.81 | 2.92 | 0.01 | 0.00 | 0.00 | 0.05 | 0.03 | 0.00 |
| 11 | 1.09 | 0.00 | - | 1.83 | 2.93 | 0.01 | 0.00 | 0.00 | 0.04 | 0.03 | 0.00 |
| 12 | 1.08 | 0.00 | - | 1.85 | 2.94 | 0.01 | 0.00 | 0.00 | 0.03 | 0.03 | 0.00 |
| 13 | 1.04 | 0.00 | - | 1.93 | 2.97 | 0.01 | 0.00 | 0.00 | 0.00 | 0.01 | 0.01 |
| 14 | 1.02 | 0.00 | - | 1.96 | 2.98 | 0.01 | 0.00 | 0.00 | 0.00 | 0.00 | 0.00 |
| 15 | 1.07 | 0.00 | - | 1.88 | 2.95 | 0.01 | 0.00 | 0.00 | 0.02 | 0.02 | 0.00 |
| 16 | 0.99 | 0.00 | - | 2.00 | 2.99 | 0.01 | 0.00 | 0.00 | 0.00 | 0.00 | 0.00 |
| 17 | 0.99 | 0.00 | - | 2.00 | 2.99 | 0.01 | 0.00 | 0.00 | 0.00 | 0.00 | 0.00 |
| 18 | 1.13 | 0.00 | - | 1.76 | 2.89 | 0.01 | 0.00 | 0.00 | 0.07 | 0.05 | 0.00 |

**Table 7.** *Cont.*

| # | Sample | Mineral | $SiO_2$ | $TiO_2$ | $Al_2O_3$ | $Cr_2O_3$ | FeO | MnO | MgO | CaO | $Na_2O$ | $K_2O$ | Total |
|---|---|---|---|---|---|---|---|---|---|---|---|---|---|
| 19 | 1.13 | 0.00 | - | 1.77 | 2.90 | 0.01 | 0.00 | | 0.00 | | 0.06 | 0.05 | 0.00 |
| 20 | 1.05 | 0.00 | - | 1.90 | 2.95 | 0.01 | 0.00 | | 0.00 | | 0.02 | 0.03 | 0.00 |
| 21 | 1.11 | 0.00 | - | 1.80 | 2.91 | 0.01 | 0.00 | | 0.00 | | 0.05 | 0.05 | 0.00 |
| 22 | 1.01 | 0.00 | - | 1.97 | 2.98 | 0.01 | 0.00 | | 0.00 | | 0.01 | 0.01 | 0.00 |
| 23 | 1.00 | 0.00 | - | 2.00 | 3.00 | 0.01 | 0.00 | | 0.00 | | 0.00 | 0.00 | 0.00 |
| 24 | 1.00 | 0.00 | - | 2.00 | 3.00 | 0.01 | 0.00 | | 0.00 | | 0.00 | 0.00 | 0.00 |
| 25 | 1.00 | 0.00 | - | 1.98 | 2.99 | 0.01 | 0.00 | | 0.00 | | 0.00 | 0.01 | 0.00 |
| 26 | 1.10 | 0.00 | - | 1.81 | 2.91 | 0.01 | 0.00 | | 0.00 | | 0.05 | 0.04 | 0.00 |
| 27 | 1.00 | 0.00 | - | 2.00 | 3.00 | 0.00 | 0.00 | | 0.00 | | 0.00 | 0.00 | 0.00 |
| 28 | 1.02 | 0.00 | - | 1.97 | 2.99 | 0.00 | 0.00 | | 0.00 | | 0.00 | 0.01 | 0.00 |

Note. Results of electron-microprobe analyses conducted by wavelength-dispersive spectrometry are listed in weight %. Phl: phlogopite. Apfu: atoms per formula unit based on 22 oxygens for phlogopite and 5 oxygens for $Al_2SiO_5$. n.d.: not detected (below detection limits).

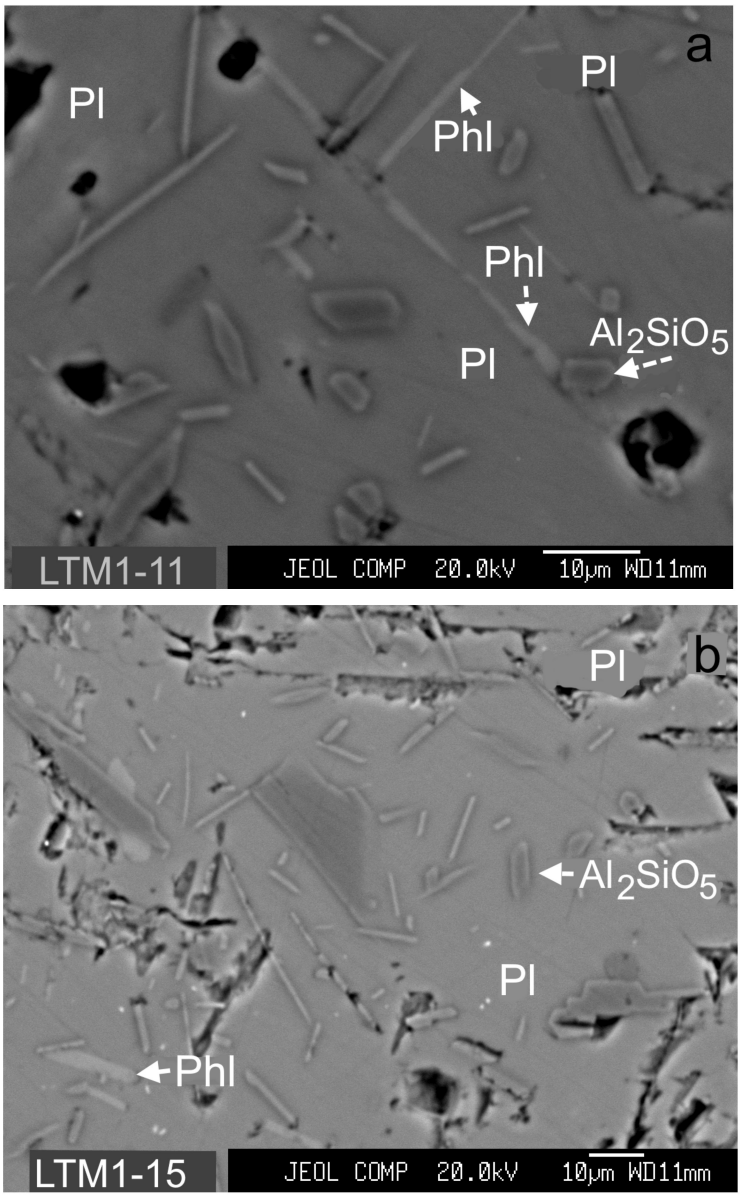


**Figure 11.** (**a**,**b**). Micrometer-sized lamellae and inclusions of phlogopite (Phl) and $Al_2SiO_5$ hosted by plagioclase (Pl) which occurs at the margin of grains of orthopyroxene in the Lotmvara-I sill. The location of these samples, Ltm1-11 and 15 (Figure 6a,c), is shown in Figure 1.

**Table 8.** Compositions of accessory grains of chlorapatite, rutile and zircon in the orthopyroxenite zone of the Lotmvara-I sill, Kola Peninsula.

| # | Sample | Mineral | $P_2O_5$ | $SiO_2$ | $TiO_2$ | $ZrO_2$ | $HfO_2$ | $ThO_2$ | $Al_2O_3$ | $Cr_2O_3$ | $V_2O_3$ | $La_2O_3$ | $Ce_2O_3$ | $Nd_2O_3$ | $Y_2O_3$ |
|---|---|---|---|---|---|---|---|---|---|---|---|---|---|---|---|
| 1 | LTM1-15 Ap1 | Clap | 41.41 | 0.18 | n.d. | n.d. | n.d. | n.d. | n.d. | n.d. | n.d. | 0.14 | 0.34 | 0.05 | n.d. |
| 2 | LTM1-15 Ap2 | - | 41.20 | 0.20 | n.d. | n.d. | n.d. | n.d. | n.d. | n.d. | n.d. | 0.16 | 0.33 | 0.08 | n.d. |
| 3 | LTM1-15 Ap3 | - | 41.31 | 0.13 | n.d. | n.d. | n.d. | n.d. | n.d. | n.d. | n.d. | 0.10 | 0.27 | 0.08 | n.d. |
| 4 | LTM1-14 Rt 1 1 | Rt | n.d. | n.d. | 96.59 | n.d. | n.d. | n.d. | 0.00 | 0.96 | 0.15 | n.d. | n.d. | n.d. | n.d. |
| 5 | LTM1-14 Rt 1 2 | - | n.d. | n.d. | 96.80 | n.d. | n.d. | n.d. | 0.02 | 0.92 | 0.10 | n.d. | n.d. | n.d. | n.d. |
| 6 | LTM1-14 Rt 2 1 | - | n.d. | n.d. | 94.79 | n.d. | n.d. | n.d. | 0.00 | 0.84 | 0.16 | n.d. | n.d. | n.d. | n.d. |
| 7 | LTM1-14 Rt 2 2 | - | n.d. | n.d. | 94.48 | n.d. | n.d. | n.d. | 0.02 | 0.85 | 0.16 | n.d. | n.d. | n.d. | n.d. |
| 8 | LTM1-14 Rt 3 1 | - | n.d. | n.d. | 94.86 | n.d. | n.d. | n.d. | 0.00 | 0.92 | 0.15 | n.d. | n.d. | n.d. | n.d. |
| 9 | LTM1-14 Rt 3 2 | - | n.d. | n.d. | 96.56 | n.d. | n.d. | n.d. | 0.00 | 0.97 | 0.30 | n.d. | n.d. | n.d. | n.d. |
| 10 | LTM1-15 Rt 1 1 | - | n.d. | n.d. | 97.63 | n.d. | n.d. | n.d. | 0.02 | 1.10 | 0.12 | n.d. | n.d. | n.d. | n.d. |
| 11 | LTM1-15 Rt 1 2 | - | n.d. | n.d. | 97.38 | n.d. | n.d. | n.d. | 0.03 | 1.03 | 0.20 | n.d. | n.d. | n.d. | n.d. |
| 12 | LTM1-15 Rt 2 1 | - | n.d. | n.d. | 96.47 | n.d. | n.d. | n.d. | 0.01 | 1.31 | 0.14 | n.d. | n.d. | n.d. | n.d. |
| 13 | LTM1-15 Rt 2 2 | - | n.d. | n.d. | 96.51 | n.d. | n.d. | n.d. | 0.00 | 1.30 | 0.11 | n.d. | n.d. | n.d. | n.d. |
| 14 | LTM1-15 Rt 3 1 | - | n.d. | n.d. | 97.34 | n.d. | n.d. | n.d. | 0.01 | 1.11 | 0.13 | n.d. | n.d. | n.d. | n.d. |
| 15 | LTM1-15 Rt 3 2 | - | n.d. | n.d. | 96.86 | n.d. | n.d. | n.d. | 0.00 | 1.21 | 0.09 | n.d. | n.d. | n.d. | n.d. |
| 16 | LTM1-15 Rt 4 1 | - | n.d. | n.d. | 96.49 | n.d. | n.d. | n.d. | 0.01 | 1.16 | 0.21 | n.d. | n.d. | n.d. | n.d. |
| 17 | LTM1-15 Rt 4 2 | - | n.d. | n.d. | 96.62 | n.d. | n.d. | n.d. | 0.00 | 1.10 | 0.15 | n.d. | n.d. | n.d. | n.d. |
| 18 | LTM1-15 Zrn 1 | Zrn | n.d. | 31.86 | n.d. | 65.98 | 1.29 | 0.23 | n.d. | n.d. | n.d. | n.d. | 0.03 | n.d. | 0.12 |
| 19 | LTM1-15 Zrn 2 | - | n.d. | 31.96 | n.d. | 65.87 | 1.57 | 0.30 | n.d. | n.d. | n.d. | n.d. | 0.04 | n.d. | 0.09 |
| 20 | LTM1-15 Zrn 3 | - | n.d. | 31.94 | n.d. | 65.93 | 1.54 | 0.32 | n.d. | n.d. | n.d. | n.d. | 0.06 | n.d. | 0.10 |
| 21 | LTM1-15 Zrn 4 | - | n.d. | 31.98 | n.d. | 65.66 | 1.52 | 0.45 | n.d. | n.d. | n.d. | n.d. | 0.00 | n.d. | 0.13 |
| 22 | LTM1-15 Zrn 5 | - | n.d. | 31.63 | n.d. | 65.56 | 1.27 | 0.23 | n.d. | n.d. | n.d. | n.d. | 0.06 | n.d. | 0.11 |

| # | FeO | MnO | MgO | CaO | SrO | ZnO | $Na_2O$ | $K_2O$ | F | Cl | Total |
|---|---|---|---|---|---|---|---|---|---|---|---|
| 1 | n.d. | n.d. | n.d. | 54.89 | 0.20 | n.d. | 0.10 | n.d. | 0.19 | 5.52 | 101.68 |
| 2 | n.d. | n.d. | n.d. | 55.06 | 0.20 | n.d. | 0.03 | n.d. | 0.03 | 6.70 | 102.46 |
| 3 | n.d. | n.d. | n.d. | 54.28 | 0.16 | n.d. | 0.02 | n.d. | 0.25 | 4.70 | 100.12 |
| 4 | 0.32 | 0.03 | 0.07 | n.d. | n.d. | n.d. | n.d. | n.d. | n.d. | n.d. | 98.11 |
| 5 | 0.36 | 0.02 | 0.06 | n.d. | n.d. | 0.03 | n.d. | n.d. | n.d. | n.d. | 98.33 |
| 6 | 0.37 | n.d. | 0.02 | n.d. | n.d. | 0.07 | n.d. | n.d. | n.d. | n.d. | 96.25 |
| 7 | 0.35 | 0.01 | 0.05 | n.d. | n.d. | 0.01 | n.d. | n.d. | n.d. | n.d. | 95.95 |
| 8 | 0.26 | n.d. | 0.07 | n.d. | n.d. | 0.06 | n.d. | n.d. | n.d. | n.d. | 96.32 |
| 9 | 0.32 | n.d. | 0.03 | n.d. | n.d. | 0.04 | n.d. | n.d. | n.d. | n.d. | 98.22 |
| 10 | 0.25 | 0.01 | 0.04 | n.d. | n.d. | 0.07 | n.d. | n.d. | n.d. | n.d. | 99.25 |
| 11 | 0.24 | n.d. | 0.01 | n.d. | n.d. | 0.05 | n.d. | n.d. | n.d. | n.d. | 98.96 |
| 12 | 0.29 | n.d. | 0.08 | n.d. | n.d. | n.d. | n.d. | n.d. | n.d. | n.d. | 98.30 |
| 13 | 0.28 | n.d. | 0.03 | n.d. | n.d. | 0.04 | n.d. | n.d. | n.d. | n.d. | 98.26 |
| 14 | 0.29 | 0.01 | 0.12 | n.d. | n.d. | 0.01 | n.d. | n.d. | n.d. | n.d. | 99.03 |
| 15 | 0.28 | 0.01 | 0.05 | n.d. | n.d. | n.d. | n.d. | n.d. | n.d. | n.d. | 98.50 |
| 16 | 0.26 | n.d. | n.d. | n.d. | n.d. | 0.04 | n.d. | n.d. | n.d. | n.d. | 98.16 |
| 17 | 0.23 | 0.01 | n.d. | n.d. | n.d. | 0.01 | n.d. | n.d. | n.d. | n.d. | 98.12 |
| 18 | n.d. | n.d. | n.d. | n.d. | n.d. | n.d. | n.d. | n.d. | n.d. | n.d. | 99.59 |
| 19 | n.d. | n.d. | n.d. | n.d. | n.d. | n.d. | n.d. | n.d. | n.d. | n.d. | 99.83 |
| 20 | n.d. | n.d. | n.d. | n.d. | n.d. | n.d. | n.d. | n.d. | n.d. | n.d. | 99.92 |
| 21 | n.d. | n.d. | n.d. | n.d. | n.d. | n.d. | n.d. | n.d. | n.d. | n.d. | 99.74 |
| 22 | n.d. | n.d. | n.d. | n.d. | n.d. | n.d. | n.d. | n.d. | n.d. | n.d. | 98.89 |

Note. Results of electron-microprobe analyses conducted by wavelength-dispersive spectrometry are listed in weight %. Clap: chlorapatite; Rt: rutile (or its trimorph); Zrn: zircon. n.d.: not detected or not analyzed. The following elements were sought, but not detected: Pr in Clap, Rt, and Zrn; Yb and U in Zrn; Ni in Rt. Totals in Clap were corrected for Cl≡O and F≡O.

The orthopyroxene grains have similar compositions: $Wo_{2.8–3.1}En_{82.4–83.3}Fs_{13.8–14.4}Aeg_{0.1–0.3}$; Mg# 81.8–84.1 (sample LTM1-11: #1-5 in Table 1), and $Wo_{2.5–3.2}En_{82.3–83.6}Fs_{13.7–14.2}Aeg_{0–0.3}$; Mg# 84.4–85.9 (LTM1-15: #19–25 in Table 1). The associated amphiboles correspond to tremolite and anthophyllite (#1–5 and 23–26 in Table 2). Zoned grains of plagioclase vary in composition: $Or_{0.1–1.4}Ab_{46.9–72.7}An_{26.8–52.7}$ (#1–9 in Table 3; LTM1-11) and $Or_{0–0.2}Ab_{71.0–81.5}An_{18.4–28.9}$ (#1–15 in Table 3; LTM1-15). The maximum An content is close to 50 mol.%, as is observed in $An_{48.5}$ in the Lyavaraka complex [6] and other suites of the Serpentine Belt. Compositions of accessory grains of chromian spinel yield Mg# values in the ranges 22.2–28.1 (#1–6) and 26.7–29.9 (#13–18 in Table 4), which overlap in the orthopyroxenite specimens. Other accessories are Cl-rich rutile and zircon (Table 8).

### *3.5. The Observed Sequences of Crystallization*

The three examples of the corona texture are thus recorded in complexes in the Serpentinite Belt. The first example involves the most primitive association observed in a fine-grained harzburgite of the Chapesvara-I sill. These coronas are composite and exhibit the following sequence (core → rim) of their formation: Ol → Opx → Cpx → Pl → Amp (aluminous, sodic-calcic). The second occurrence, indicative of the order Opx →

Cpx → Amp → Pl → Qz, is documented in an orthopyroxenite rock in the Lotmvara-I sill. The third occurrence with symplectite-type coronas is developed in a plagioclase-bearing orthopyroxenite in the Zone of Recurrent Ol + Cpx + Pl (III) in the Lyavaraka complex. The latter textures formed in contact with grains of Pl and point to the following order of crystallization: Cpx → Amp (aluminous hornblende) + Qz (symplectitic).

## 4. Discussion

The corona texture can clearly develop at different stages of crystallization of the ultrabasic complexes of the Serpentinite Belt. Initially, it forms during the crystallization of the olivine–orthopyroxene paragenesis; the Mg# index of the olivine core in harzburgite is 86–87, as illustrated in the differentiated Chapesvara-I sill. In the Lotmvara-I complex, the corona involved a more differentiated (evolved) orthopyroxenite; the core of orthopyroxene has a Mg# in the range 79–83.5. The third example, at Lyavaraka, associated with primocrysts of clinopyroxene and late grains of plagioclase, is characterized by an abundance of quartz present in a symplectitic association. In all of these occurrences, grains of plagioclase (up to 55 mol.% An) formed at advanced to late stages.

In the three complexes of the Serpentinite Belt, a corona texture developed in pristine igneous rocks (Figure 6a–e). Its presence reflects special conditions of crystallization involving (1) rapid cooling in a subvolcanic setting and (2) an inferred buildup of $H_2O$ and other volatile species that have become saturated in the Al-undepleted komatiitic magma. Degassing likely contributed to the forced crystallization. Local reactions of the aqueous fluid with grains of early pyroxene and late plagioclase caused the deposition of an amphibole rim, induced deuterically at an advanced stage of crystallization, in the external portion of the corona. Clearly, the corona texture in such an environment cannot be ascribed to processes of regional metamorphism.

The recognition of the corona texture in ultrabasic suites of the Serpentinite Belt points to their petrogenetic relationship with drusites of the Belomorian complex in the Karelia–Kola region in the northeastern Fennoscandian Shield. We believe that a complementary belt and related megastructure developed synchronously with the SB–TB structure, extending linearly from the Tulppio group toward the synchronous Belomorian (or Kovdozero) complex close to the Kandalaksha paleorift system. We propose that suites of the southern branch of the SB, namely the Tepsi-Tundra, Urochishche Tepsi, Kareka-Tundra, Yanisvaara, and Perchatka suites, likely belong to the complementary belt being proposed. In general, mean whole-rock compositions of the Belomorian drusite series have greater $SiO_2$ contents, considered to reflect a more siliceous (boninite-like) parental melt. This enrichment can be attributed to the "dispersed intrusive magmatism" of the Lapland–Belomorian mobile belt [11,21]. These series of Paleoprotetorozoic ages thus seem to become progressively more evolved in a southeasterly direction and along the strike of the complementary belt. We hypothesize that in some cases, corona development in the Belomorian drusite suites could be the result of autometasomatic reactions rather than regional metamorphism.

It has been argued [22] that the barren characteristics of the Belomorian drusite suites are related to the low contents of fluid in these ultramafic–mafic rocks. As an alternative explanation, the major reason for the relatively low ore potential could be the relatively small volumes of their parental magma. Occurrences of Pd–Pt mineralization [23] are known in the Kovdozero complex, a type locality for these rocks. Our results indicate the existence of elevated levels of volatile components in suites of the Serpentinite Belt. Occurrences of Ru–Os–Ir mineralization exist in chromite zones of the Pados-Tundra complex in the Serpentinite belt [24]. It follows that the larger members of the drusite suite should be searched for deposits of platinum-group elements in relation to chromite or low-sulfide zones.

In addition, magma mixing processes are inferred to cause reactions of the type Pl + Si-rich melt → Amp + Qz and Cpx + Si-rich melt → Amp + Pl + Qz in gabbroic layered intrusions of the Sichuan Province, southwestern China [25,26], and in other localities. In our case, there is no evidence for a new magma influx, however. Indeed, subordinate

amounts of amphiboles or other species of hydrous silicates (and minor quartz in Ol-free rocks) are not unusual in the interstices between grains of early silicates in mafic-ultramafic complexes. They are late products of fractional crystallization and normal differentiation in single batches of magma. We infer that the corona-forming assemblage of Amp + Qz in the Serpentinite Belt developed locally as a result of small-volume deuteric (autometasomatic) alteration of early Cpx + late Pl. All of the corona-type textures are likely consequences of the complicated evolution of the subvolcanic bodies of the belt, which formed in relation to a sudden drop in temperature during rapid crystallization and degassing of a komatiitic magma under the conditions of a closed system.

*Lamellar Inclusions at Lotmvara-I and a Comparison with Lukkulaisvaara*

The associated lamellae of phlogopite and one of the trimorphs of $Al_2SiO_5$ generally display a disoriented distribution in host grains of interstitial plagioclase (Figure 11b) in the sill. These inclusions thus likely nucleated in the melt prior to the host phase during a final stage of crystallization of pockets of remaining $H_2O$-bearing melt enriched in Al, K, and Na. Degassing of the melt would explain a preferential loss of Na and the local saturation of the melt in phlogopite and $Al_2SiO_5$ crystallites. This mode of occurrence resembles an atypical assemblage reported from the Lukkalaisvaara layered intrusion, northern Russian Karelia [27], which is coeval with suites of the Serpentinite Belt, cf. [8,15]. The preferred orientation of the crystallites (Figure 11a, upper part) could be explained by their migration from the melt to the growth surfaces of the host plagioclase.

At Lukkulaisvaara, a diverse assemblage of high-aluminum species was documented in a pegmatitic orthopyroxenite–gabbronorite rock rich in platinum-group elements (especially in Pd, Pt) and Ag, and associated with base-metal sulfides (mostly chalcopyrite with subordinate bornite, pentlandite, and millerite). The PGE–Ag mineralized pods and stringers occur close to the center of a sill-like body of microgabbronorite hosted by mafic rocks (mostly gabbronorite) of the layered series [27–29]. This rock, shown schematically in Figure 12a,b, formed in situ as a result of the crystallization of isolated volumes of $H_2O$-saturated melt during the crystallization of the sill. The Al-enriched assemblage includes an $Al_2SiO_5$ phase in intergrowth with microcrystalline staurolite, ferropargasitic to tschermakitic amphiboles, with a variant of chloro-ferro-pargasite having up to 4.5 wt.% Cl, almandine, phlogopite, hercynite, corundum, and an AlO(OH) phase [27]. Grains of Cl-enriched amphiboles and phlogopite are highly abundant, with numerous inclusions of Cl-rich amphiboles in grains of base-metal sulfides, platinum-group minerals, and even in staurolite. The Amp–Alm–St–$Al_2SiO_5$ assemblage likely formed at a temperature range of 560 to 670 °C at a deuteric stage and at the expense of igneous orthopyroxene and plagioclase [27].

Therefore, close similarities appear to exist between these occurrences at Lotmvara-I and Lukkulaisvaara: (1) the Al-enriched assemblages, including the $Al_2SiO_5$ phase, are intimately associated with grains of primary plagioclase in specimens of Pl-bearing orthopyroxenite; (2) these occurrences formed from portions of $H_2O$-saturated melt enriched in Cl. The presence of Cl at Lotmvara-I is indicated by the crystallization of chlorapatite: Cl 66.1–92.9 OH 6.3–27.3 F 0.8–6.6, if recalculated for a total of 100 mol.% (#1–3 in Table 8). (3) In both cases, these occurrences are closely related to the crystallization of the sill-like bodies, which thus imply effects of rapid crystallization following selective degassing, with the possibility of metastable crystallization of $Al_2SiO_5$ and other uncommon phases at the deuteric stage. In addition, these observations imply that garnet, $Al_2SiO_5$, and other aluminous species can likely be deposited, under special conditions, as components of corona-type textures in drusites or related rocks.

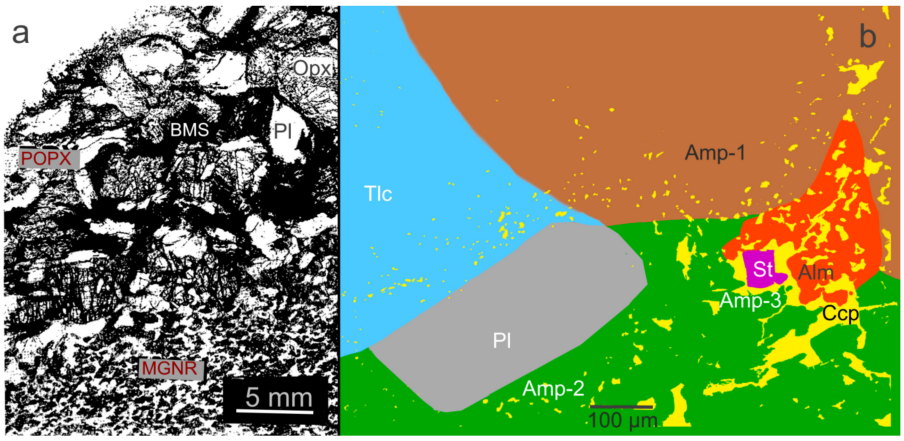


**Figure 12.** (**a**) Shows an example of pegmatitic gabbronorite grading to plagioclase-bearing orthopyroxenite (POPX) observed in polished section, cf. [27]. This rock, highly enriched in Pd-Pt-(Ag), is composed of orthopyroxene (Opx), plagioclase (Pl), and base-metal sulfides (BMS) of the chalcopyrite-(Ccp)-bornite-millerite assemblage. The POPX rock is hosted by a sill-like body of microgabbronorite, MGNR, which is present in direct contact in (**a**). (**b**) is a false-color image displaying, schematically, the previously reported occurrence [27]. Grains of talc (Tlc) and an anthophyllite-related amphibole (Amp-1) formed as a result of deuteric alteration at the expense of igneous orthopyroxene ($En_{75–77}$). The peraluminous assemblage includes alumino- and chlorian varieties of tschermakite (Amp2 and 3, respectively), an almandine garnet (Alm), and a tiny grain of staurolite (St). These minerals of the Al-rich assemblage are intimately associated with a large grain of late-magmatic plagioclase: $An_{63}$ (Pl).

## 5. Conclusions

1. The presence of a corona texture is documented for the first time in ultrabasic rocks in three members of the Serpentinite Belt on the Kola Peninsula. It occurs in a fine-grained harzburgite of the Chapesvara-I sill, in which the following order of crystallization is recognized in the corona: Ol → Opx → Cpx → Pl → Amp (aluminous sodic-calcic). In the second occurrence, the sequence Opx → Cpx → Amp → Pl → Qz is inferred in an orthopyroxenite rock in the Lotmvara-I sill. A symplectitic corona developed in the third occurrence exists in a plagioclase-bearing orthopyroxenite in the Zone of Recurrent Ol + Cpx + Pl (III) in the Lyavaraka complex, in which the inferred order is: Cpx → Amp (aluminous hornblende) + symplectitic Qz, formed in direct contact with grains of Pl.
2. We believe that these corona-type textures are not related to processes of regional metamorphism. They occur in fresh rocks and reflect different stages in the history of the Serpentinite Belt, from an early stage involving the nucleation of the olivine "core" (Mg# Ol = 87) at Chapesvara-I to late stages related to the deposition of the symplectitic association of Amp + Qz in the Pl-bearing orthopyroxenite at Lyavaraka. All these examples likely formed as consequences of the two most important circumstances. (i) Physicochemical conditions were unsteady and changed drastically in relation to rapid and heterogeneous cooling in a shallow setting during crystallization of the subvolcanic complexes. (ii) An intrinsic enrichment in $H_2O$ and other volatiles in the komatiitic magma was important to give rise to fluid-saturated media at advanced stages of crystallization, which caused a deuteric deposition of amphibole rims as a result of reactions with grains of pyroxenes and late plagioclase.
3. Our findings on the presence of corona-type textures in complexes of the Serpentinite Belt imply close relationships between the ultrabasic suites of this belt (and the entire SB–TB structure) and drusites of the Belomorian complex in the Karelia–Kola region of the northeastern Fennoscandian Shield. A complementary belt and megastructure synchronous to the SB–TB may well exist, which is proposed to extend linearly from

some suites of the Tulppio group toward the synchronous Belomorian (or Kovdozero) complex close to the Kandalaksha paleorift system.

4. Our results and observations may stimulate further attempts to re-examine the origin of the corona textures in mafic-ultramafic complexes of the Belomorian drusite complex. The development of some corona textures could have resulted from autometasomatic processes rather than regional metamorphism.
5. Unusual occurrences of lamellar inclusions of phlogopite and $Al_2SiO_5$ are documented in host grains of plagioclase in specimens of orthopyroxenite in the Lotmvara-I sill. These inclusions likely formed from late portions of remaining melt enriched in Al, K, Na, $H_2O$, and Cl and could reflect the consequences of selective degassing of the late melt, made peraluminous by the loss of Na and other components. The abundance of Cl in the late fluid is evident from the documented occurrence of chlorapatite, the first example so far in the Serpentinite Belt.
6. The presence of intrinsic volatiles, Cl, F, $CO_2$, and especially magmatic $H_2O$ lowered the liquidus and decreased the density and viscosity of the highly magnesian melt, which enhanced its ability to attain a shallow level in the crust.

**Author Contributions:** The authors wrote the article together. A.Y.B.: investigations, interpretations, writing; A.A.N.: writing, discussions; V.N.K.: analytical work, writing; R.F.M.: conclusions, writing. All authors have read and agreed to the published version of the manuscript.

**Funding:** This study was supported by the Russian Science Foundation (grant #22-27-00419).

**Data Availability Statement:** All the data are provided in the article.

**Acknowledgments:** We thank four anonymous reviewers for their constructive comments. A.Y.B. gratefully acknowledges an additional support of this investigation by Cherepovets State University. We thank the staff of the Russian Geological Research Institute (VSEGEI) and the Federal Subsoil Resources Management Agency (Rosnedra) for providing access to sets of geological maps. V.N.K. acknowledges that the present work was also conducted on the state assignment of IGM SB RAS, supported by the Ministry of Science and Higher Education of the Russian Federation.

**Conflicts of Interest:** The authors declare no conflict of interest.

## References

1. Ogilvie, P.; Gibson, R.L. Arrested development—A comparative analysis of multilayer corona textures in high-grade metamorphic rocks. *Solid Earth* **2017**, *8*, 93–135. [CrossRef]
2. Turner, S.P.; Stüwe, K. Low-pressure corona textures between olivine and plagioclase in unmetamorphosed gabbros from Black Hill, South Australia. *Miner. Mag.* **1992**, *56*, 503–509. [CrossRef]
3. Helmy, H.M.; Yoshikawa, M.; Shibata, T.; Arai, S.; Tamura, A. Corona structure from arc mafic-ultramafic cumulates: The role and chemical characteristics of late-magmatic hydrous liquids. *J. Miner. Petrol. Sci.* **2008**, *103*, 333–344. [CrossRef]
4. Barkov, A.Y.; Korolyuk, V.N.; Barkova, L.P.; Martin, R.F. Double-front crystallization in the Chapesvara ultramafic subvolcanic complex, Serpentinite Belt, Kola Peninsula, Russia. *Minerals* **2019**, *10*, 14. [CrossRef]
5. Barkov, A.Y.; Nikiforov, A.A.; Barkova, L.P.; Korolyuk, V.N.; Martin, R.F. Zones of PGE–chromite mineralization in relation to crystallization of the Pados-Tundra ultramafic complex, Serpentinite Belt, Kola Peninsula, Russia. *Minerals* **2021**, *11*, 68. [CrossRef]
6. Barkov, A.Y.; Nikiforov, A.A.; Korolyuk, V.N.; Martin, R.F. The Lyavaraka ultrabasic complex, Serpentinite Belt, Kola Peninsula, Russia. *Geosciences* **2022**, *12*, 323. [CrossRef]
7. Barkov, A.Y.; Nikiforov, A.A.; Barkova, L.P.; Izokh, A.E.; Korolyuk, V.N. Komatiitic subvolcanic rocks in the mount Khanlauta massif, Serpentinite Belt, Kola Peninsula. *Russ. Geol. Geoph.* **2022**, *63*, 981–1000. [CrossRef]
8. Serov, P.A.; Bayanova, T.B.; Steshenko, E.N.; Kunakkuzin, E.L.; Borisenko, E.S. Metallogenic setting and evolution of the Pados-Tundra Cr-bearing ultramafic complex, Kola Peninsula: Evidence from Sm–Nd and U–Pb isotopes. *Minerals* **2020**, *10*, 186. [CrossRef]
9. Melezhik, V.A.; Hanski, E.J. Palaeotectonic and palaeogeographic evolution of Fennoscandia in the Early Palaeoproterozoic. In *Reading the Archive of Earth's Oxygenation. 1. The Palaeoproterozoic of Fennoscandia as Context for the Fennoscandian Arctic Russia—Drilling Early Earth Project*; Melezhik, V.A., Prave, A., Fallick, A., Kump, L., Strauss, H., Lepland, A., Hanski, E.J., Eds.; Springer: Berlin/Heidelberg, Germany, 2013. [CrossRef]

10. Hanski, E.J. Evolution of the Palaeoproterozoic (2.50–1.95 Ga) Non-Orogenic Magmatism in the Eastern Part of the Fennoscandian Shield. In *Reading the Archive of Earth's Oxygenation. 1. The Palaeoproterozoic of Fennoscandia as Context for the Fennoscandian Arctic Russia—Drilling Early Earth Project*; Melezhik, V.A., Prave, A., Fallick, A., Kump, L., Strauss, H., Lepland, A., Hanski, E.J., Eds.; Springer: Berlin/Heidelberg, Germany, 2013. [CrossRef]
11. Sharkov, E.V.; Krassivskaya, I.S.; Chistyakov, A.V. Belomorian drusite (coronite) complex, Baltic Shield, Russia: An example of dispersed intrusive magmatism in early Paleoproterozoic mobile zones. *Russ. J. Earth Sci.* **2004**, *6*, 185–215. [CrossRef]
12. Fedorov, E.S. On a new group of igneous rocks. *Proc. Moscow Agricult. Inst.* **1896**, *1*, 12–29. (In Russian)
13. Larikova, T.L. Genesis of drusitic (corona) textures around olivine and orthopyroxene during metamorphism of gabbroic rocks in northern Belomorie, Karelia. *Petrology* **2000**, *8*, 384–401.
14. Sharkov, E.V.; Snyder, G.A.; Taylor, L.A.; Zinger, T.F. An Early Proterozoic large igneous province in the Eastern Baltic Shield: Evidence from the mafic drusite complex, Belomorian Mobile Belt, Russia. *Int. Geol. Rev.* **1999**, *41*, 73–93. [CrossRef]
15. Amelin, Y.V.; Heaman, L.M.; Semenov, V.S. U–Pb geochronology of layered mafic intrusions in the eastern Baltic Shield: Implications for the timing and duration of Paleoproterozoic continental rifting. *Precamb. Res.* **1995**, *75*, 31–46. [CrossRef]
16. Shlayfshteyn, B.A. *The Account on Results of Additional Geological Appraisal at a Scale of 1:200,000 in the Northwestern Part of the Kola Peninsula (1981–1987 Years)*; The Central-Kola Geological Survey (expedition); "Sevzapgeologiya", the Ministry of Geology of the RSFSR: Monchegorsk, Russia, 1987; *unpublished report in Russian*.
17. Spirov, V.N. *Geological Map (1:10,000) of the Detailed Mapping Area at River Khlebnaya*; An Account of the Western Kola Geological Party for the Years 1968–1971; The Allarechensky Geological Party, North-Western Territorial Geological Department, Murmansk Geological-Prospecting Expedition, the U.S.S.R. Ministry of Geology: Murmansk, Russia, 1972; *unpublished report in Russian*.
18. Korolyuk, V.N.; Usova, L.V.; Nigmatulina, E.N. Accuracy in the determination of the compositions of main rock-forming silicates and oxides on a JXA-8100 microanalyzer. *J. Anal. Chem.* **2009**, *64*, 1042–1046. [CrossRef]
19. Morimoto, N.; Fabriès, J.; Ferguson, A.K.; Ginzburg, I.V.; Ross, M.; Seifert, F.A.; Zussman, J.; Aoki, K.; Gottardi, G. Nomenclature of Pyroxenes. *Miner. Mag.* **1988**, *52*, 535–550. [CrossRef]
20. Hawthorne, F.C.; Oberti, R.; Harlow, G.E.; Maresch, W.V.; Martin, R.F.; Schumacher, J.C.; Welch, M.D. Nomenclature of the amphibole supergroup. *Am. Miner.* **2012**, *97*, 2031–2048. [CrossRef]
21. Terekhov, E.N. Lapland–Belomorian mobile belt as an example of the root zone of the Paleoproterozoic rift system of the Baltic Shield. *Litosfera* **2007**, *6*, 15–39. (In Russian)
22. Malov, N.D. Structural-petrological and specific metallogenic features of drusites in the north-western Belomorye. *Vestn. St.-Petersburg Univ. Earth Sci.* **2015**, *7*, 73–84. (In Russian)
23. Barkov, A.Y.; Laajoki, K.V.O.; Karavaev, S.S. First Occurrences of Pd-Pt Minerals in the Kovdozero Mafic-Ultramafic Complex, NE Fennoscandian Shield. In *Mineral Deposits*; Papunen, H., Ed.; Balkema: Rotterdam, The Netherlands, 1997; pp. 393–394.
24. Barkov, A.Y.; Nikiforov, A.A.; Tolstykh, N.D.; Shvedov, G.I.; Korolyuk, V.N. Compounds of Ru–Se–S, alloys of Os–Ir, framboidal Ru nanophases, and laurite–clinochlore intergrowths in the Pados-Tundra complex, Kola Peninsula, Russia. *Eur. J. Miner.* **2017**, *29*, 613–621. [CrossRef]
25. Zhou, M.-F.; Robinson, P.T.; Lesher, C.M.; Keays, R.R.; Zhang, C.-J.; Malpas, J. Geochemistry, petrogenesis, and metallogenesis of the Panzhihua gabbroic layered intrusion and associated Fe-Ti-V-oxide deposits, Sichuan Province, SW China. *J. Petrol.* **2005**, *46*, 2253–2280. [CrossRef]
26. Zhou, M.-F.; Chen, W.T.; Wang, C.Y.; Prevec, S.A.; Liu, P.P.; Howarth, G.H. Two stages of immiscible liquid separation in the formation of Panzhihua-type Fe-Ti-V oxide deposits, SW China. *Geosci. Front.* **2013**, *4*, 481–502. [CrossRef]
27. Barkov, A.Y.; Martin, R.F.; Laajoki, K.V.O.; Alapieti, T.T.; Iljina, M.J. Paragenesis and origin of staurolite from a palladium-rich gabbronorite: An unusual occurrence from the Lukkulaisvaara layered intrusion, Russian Karelia. *Neues Jb. Mineral.—Abh.* **1999**, *175*, 191–222. [CrossRef]
28. Barkov, A.Y.; Lednev, A.I. A rhenium-molybdenum-copper sulfide from the Lukkulaisvaara layered intrusion, northern Karelia, Russia. *Eur. J. Miner.* **1993**, *5*, 1227–1234. [CrossRef]
29. Barkov, A.Y.; Martin, R.F.; Tarkian, M.; Poirier, G.; Thibault, Y. Pd-Ag tellurides from a Cl-rich environment in the Lukkulaisvaara layered intrusion, northern Russian Karelia. *Can. Miner.* **2001**, *39*, 639–653. [CrossRef]